CHAPTER 2 GRAVITY SURVEY

2 - 1 Survey Method

Figure 2-2-1 shows the flowchart of this gravity survey.

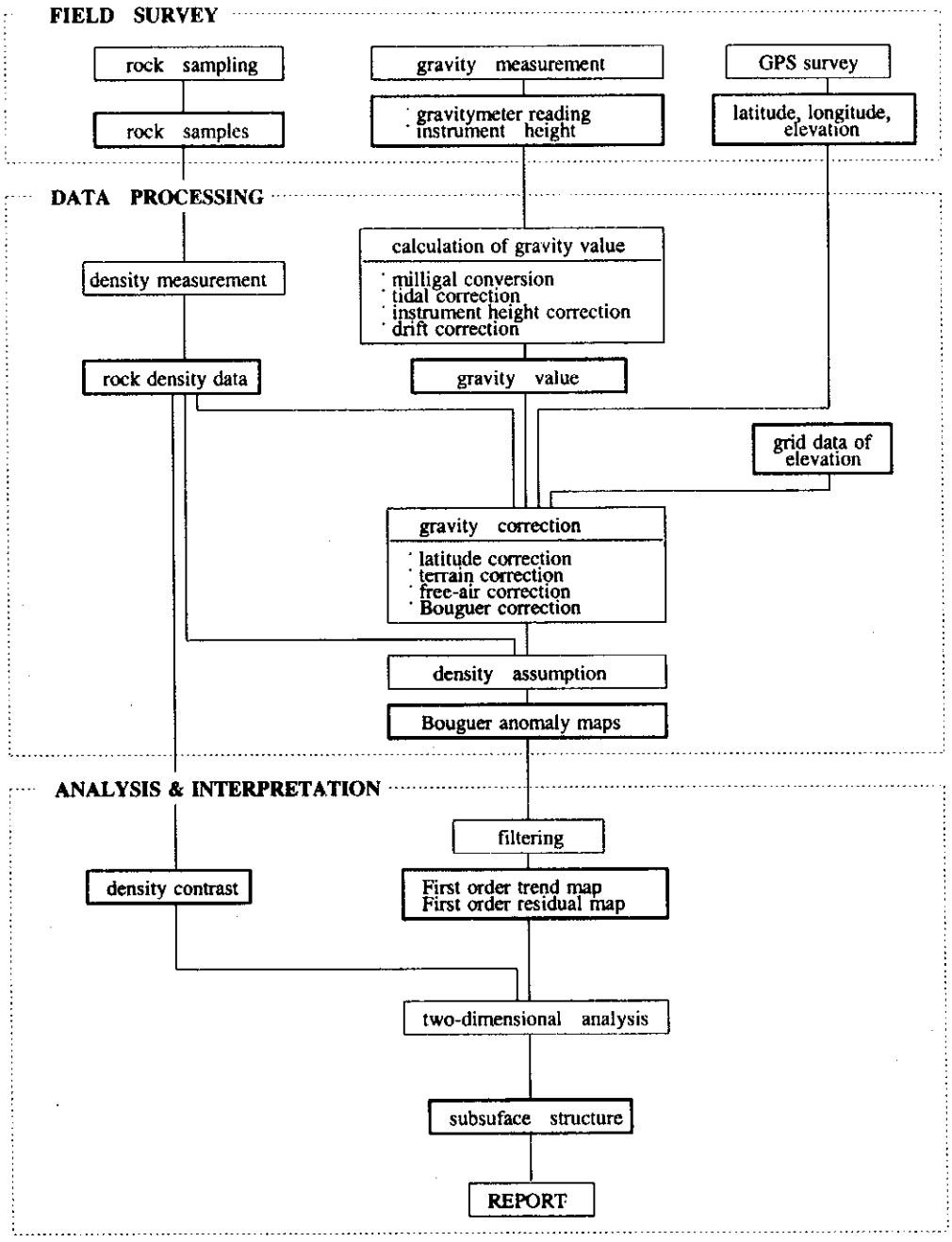

Fig.2-2-1 Flowchart of Gravity Survey

2-1-1 Field survey

(1) Gravity measurements

Gravity survey was started with more than 300 stations within an area of 500km^2 (25km E-W×20kmN-S) in the Camarones district. Additional 30 stations in a 38km^2 area on the northwestern side of the original area were added during the survey.

The final number of stations measured was 318 in the originally planned area and 31 stations in the added area. The locations of the stations are shown in Figure 2-2-2. A helicopter was used for commuting to far-off locations in the eastern, southern, and western parts of the district. The number of stations measured using helicopter amounted to 150 which constitute 43% of the total.

We used two LaCoste gravimeters with the following specifications.

Gravity meter No.	G-178	G-365
Year of manufacture	Feb. 1968	Mar. 1974
Operating range	0~7,344.88mgal	0~7,447.81mgal
Accuracy	0.02 mgal	
Size	14×15×20 cm	
Weight	8.6 kg	
Power source	12 V battery	
Manufacturer	LaCoste & Romberg (USA)	

The base station (No. 1000) for the measurements was established within the base camp of the survey team at Codpa about 1km northwest of the survey area. The gravity value (978,044.68mgal) of the base station was determined by measurement between the base station and the Chile University gravity base (g=978,480.233mgal) within the Arica Airport about 100km northwest of the survey area. The measured values are listed below.

DATE: 2000/11/24
LACOSTE G-178

No.	TIME	READING	INST. HEIGHT	*FACT	INST. COR	ETCOR	+ COR	DRIFT COR	GRVTY DIF.	GRAVITY VALUE
	H M		m	mgal	mgal	mgal	mgal	mgal	mgal	mgal
1000	8 16	1595.978	.27	1670.498	.083	-.034	1670.547	.000	-435.557	978044.676
Arica	11 39	2011.575	.27	2105.858	.083	.159	2106.101	.004	.000	978480.233
1000	17 20	1595.970	.27	1670.490	.083	-.091	1670.537	.010	-435.557	978044.676
					DRIFT RATE =		-.00109 mgal/hour			

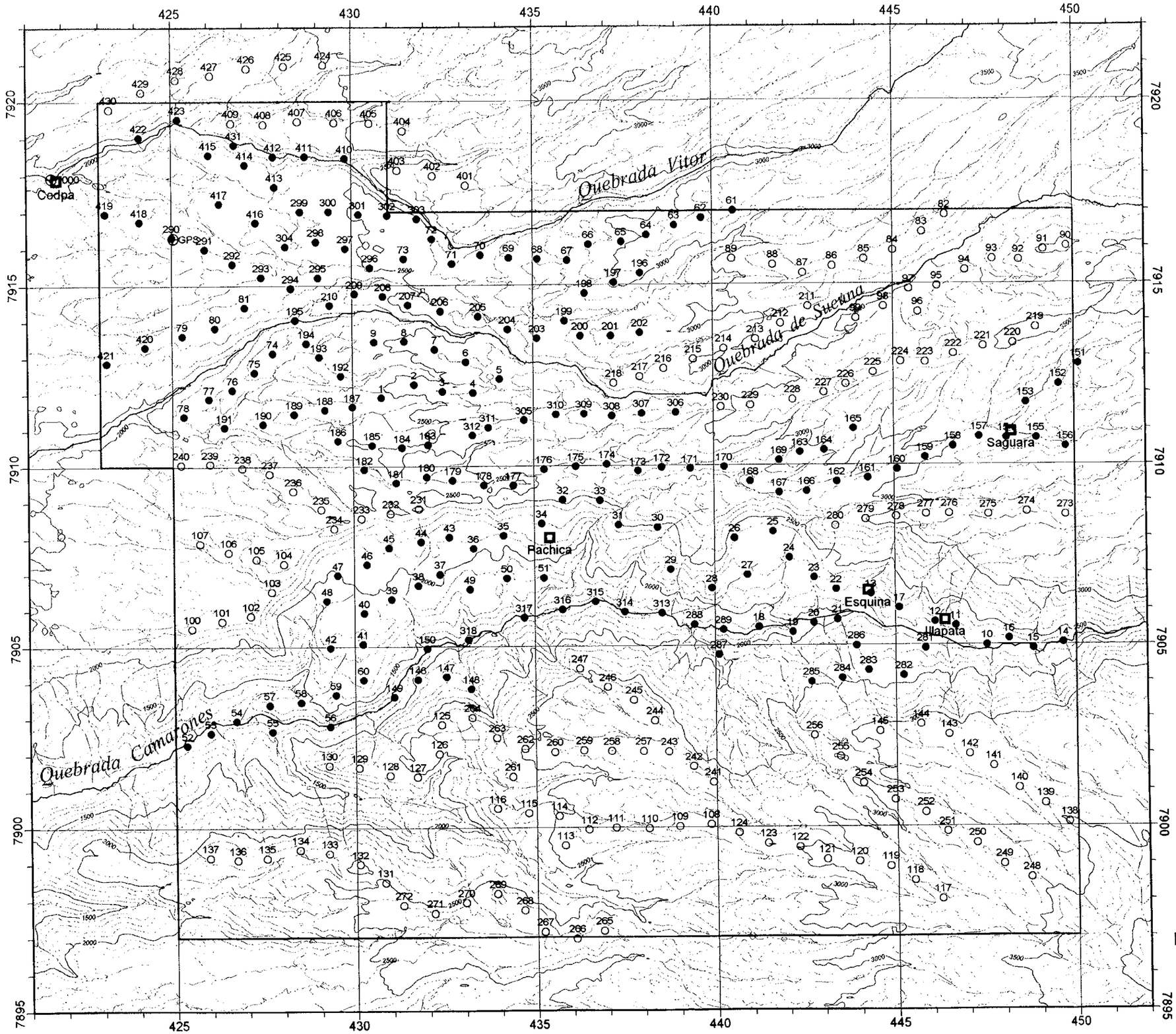

LEGEND

○ By Helicopter

● By Car

Fig.2-2-2
Location of Gravity Station

(2) Leveling

Static GPS(Global Positioning System) survey was used for measurement of the location and elevation of each station. There are two positioning methods for static GPS survey, namely single positioning with one receiver and differential positioning using two receivers. For the present survey, differential positioning with high accuracy of centimeter order was used . In this method, signals are received simultaneously at two points, the fixed point (base station) and the measuring point, and the difference of the elevation and the relative location of the two points is measured. Three Trimble 4600LS GPS surveyers by Trimble Navigation Ltd. of USA were used. One was for the base station and two for measuring points.

The GPS base station was set at the northwest edge of the survey area about 3.5km southeast of Codpa. This point is the same as the gravity station No.290. The location and elevation of the GPS base station were determined by GPS survey from the triangulation point "Garza" located about 17km west-northwest.

(3) Density measurements of rock samples

Density of 86 rock samples collected in the survey area was measured. The locality of the samples is shown in Figure 2-2-3.

The weight of the samples under three conditions was measured and the density was calculated from the following formula.

Natural dry density = $W_1/(W_2-W_3)$

Wet density = $W_2/(W_2-W_3)$

W_1: weight of the sample in air after left in a normal room condition for a few days.

W_2: weight of the sample in air after immersed in water for about 24 hours and the surface water wiped off (wet sample).

W_3: weight of the wet sample in water.

The two kinds of density of the samples are listed in Table 2-2-1, and the average densities are shown for each formation and rock in Table 2-2-2.

It is seen from Table 2-2-2 that Quaternary agglomerate and Miocene ignimbrite forms the low-density group, while Quaternary basalt, basement rocks (Upper Cretaceous System, Upper Cretaceous~Paleogene System), and Cretaceous to Tertiary intrusive rocks form the high-density group. The difference between natural dry density and wet density of the low-density group rocks is 0.06~0.20g/cm^3, and the effective porosity is relatively large. On

Table 2-2-1 Results of rock density measurements (1/2)

Sample No.	Rock name	Density (g/cm^3)		Coordinates(km)	
		Natural dry	Wet	X	Y
1	Pumice tuff	1.91	2.02	433.648	7912.021
2	Pumice tuff	1.60	1.86	430.485	7913.279
3	Highly welded tuff	2.31	2.37	449.609	7910.606
4	Highly welded tuff	2.41	2.45	445.705	7910.368
5	Highly welded tuff	2.24	2.33	443.376	7909.613
6	Basalt	2.57	2.61	443.879	7910.975
7	Pumice tuff	1.61	1.89	438.479	7909.997
8	Highly welded tuff	2.21	2.32	432.286	7908.038
9	Highly welded tuff	2.19	2.30	431.890	7907.960
10	Agglomerate	1.95	2.13	430.485	7907.536
11	Agglomerate	1.82	1.94	429.413	7906.489
12	Pumice tuff	1.57	1.81	434.138	7908.064
13	Highly welded tuff	2.18	2.29	437.117	7914.998
14	Highly welded tuff	2.35	2.41	435.885	7914.074
15	Highly welded tuff	2.24	2.31	435.184	7913.436
16	Pumice tuff	1.93	2.10	433.676	7914.007
17	Pumice tuff	1.64	1.92	440.556	7913.238
18	Pumice tuff	1.46	1.74	439.525	7912.933
19	Pumice tuff	2.07	2.19	437.831	7912.417
20	Basalt	2.62	2.64	448.537	7913.423
21	Basalt	2.61	2.62	444.316	7912.483
22	Basalt	2.67	2.69	443.574	7912.166
23	Basalt	2.62	2.63	443.322	7912.087
24	Basalt	2.59	2.63	440.544	7911.663
25	Basalt	2.62	2.64	431.689	7908.765
26	Agglomerate	1.88	2.08	430.010	7908.595
27	Pumice tuff	1.55	1.80	427.867	7909.692
28	Basalt	2.55	2.56	426.754	7910.063
29	Pumice tuff	1.88	2.07	426.106	7909.969
30	Pumice tuff	1.70	1.94	439.868	7901.208
31	Pumice tuff	1.61	1.90	438.758	7902.453
32	Pumice tuff	1.84	2.05	436.998	7903.657
33	Highly welded tuff	2.37	2.38	438.783	7902.334
34	Basalt	2.69	2.70	436.467	7904.345
35	Basalt	2.50	2.54	448.524	7898.643
36	Pumice tuff	1.81	2.01	446.563	7899.436
37	Weakly welded tuff	1.94	2.09	446.010	7899.436
38	Weakly welded tuff	2.04	2.18	445.492	7899.753
39	Highly welded tuff	2.27	2.34	443.904	7901.592
40	Weakly welded tuff	2.11	2.22	442.926	7902.321
41	Diorite porphyry	2.66	2.67	443.998	7906.621
42	Diorite porphyry	2.67	2.68	443.998	7906.621
43	Quartz diorite	2.73	2.75	438.677	7898.074

Table 2-2-1 Results of rock density measurements (2/2)

Sample No.	Rock name	Density (g/cm^3)		Coordinates(km)	
		Natural dry	Wet	X	Y
44	Quartz diorite	2.71	2.72	438.677	7898.074
45	Quartz diorite	2.61	2.61	426.980	7918.864
46	Quartz diorite	2.58	2.58	426.980	7918.864
47	Highly welded tuff	2.18	2.25	433.345	7917.657
48	Highly welded tuff	2.35	2.38	431.227	7918.308
49	Highly welded tuff	2.37	2.42	431.585	7919.484
50	Highly welded tuff	2.30	2.37	429.731	7919.301
51	Basalt	2.64	2.64	449.556	7908.699
52	Pumice tuff	1.72	1.96	447.186	7908.846
53	Weakly welded tuff	2.05	2.21	445.309	7908.633
54	Weakly welded tuff	2.12	2.24	443.348	7908.315
55	Agglomerate	2.14	2.20	442.914	7908.765
56	Pumice tuff	1.66	1.92	445.347	7904.094
57	Highly welded tuff	2.24	2.32	445.227	7904.068
58	Agglomerate	2.04	2.18	444.938	7904.201
59	Weakly welded tuff	2.06	2.20	443.800	7904.015
60	Weakly welded tuff	2.04	2.17	442.593	7903.830
61	Rhyolitic volcaniclastics	2.56	2.58	440.015	7904.716
62	Andesitic lava / volcaniclastics	2.68	2.69	439.777	7904.993
63	Andesitic lava / volcaniclastics	2.65	2.66	439.431	7905.496
64	Andesitic lava / volcaniclastics	2.72	2.72	439.683	7905.483
65	Quartz diorite	2.59	2.60	438.545	7900.177
66	Pumice tuff	1.59	1.78	435.184	7906.200
67	Weakly welded tuff	2.04	2.18	425.233	7911.427
68	Basalt	2.62	2.63	449.144	7915.885
69	Weakly welded tuff	2.09	2.21	444.765	7914.338
70	Pumice tuff	1.85	2.05	430.023	7901.554
71	Highly welded tuff	2.37	2.45	427.376	7899.278
72	Highly welded tuff	2.42	2.45	449.688	7900.124
73	Highly welded tuff	2.65	2.66	449.688	7900.124
74	Highly welded tuff	2.67	2.69	449.027	7900.667
75	Diorite	2.80	2.80	436.586	7906.316
76	Andesitic lava / volcaniclastics	2.62	2.63	432.748	7905.074
77	Andesitic lava / volcaniclastics	2.54	2.57	433.132	7905.194
78	Highly welded tuff	2.37	2.39	429.071	7920.914
79	Highly welded tuff	2.22	2.30	425.047	7920.637
80	Quartz porphyry	2.54	2.55	435.319	7905.854
81	Quartz porphyry	2.43	2.44	438.951	7905.889
82	Quartz porphyry	2.50	2.51	434.904	7906.701
83	Quartz porphyry	2.51	2.51	435.614	7906.789
84	Quartz diorite	2.59	2.59	426.420	7918.999
85	Granodiorite	2.51	2.51	436.628	7905.977
86	Quartz diorite	2.72	2.72	439.000	7899.618

Table 2-2-2 Average Densities of Rock Sample

Age	Rock name		Average density (g/cm³)				Density (g/cm³) 1.60 1.80 2.00 2.20 2.40 2.60 2.80	No. of sample
			Natural dry		Wet			
Quaternary	Basalt		2.61		2.63			12
	Agglomerate		1.97	2.04	2.11	2.18		5
Tertiary (Neogene)	Ignimbrite	Pumice tuff / weakly welded tuff	1.83		2.03			27
		Highly welded tuff	2.33		2.39			21
Cretaceous - Early Tertiary	Rhyolitic volcaniclastics/ lava,dacitic lava/dome		2.56	2.62	2.58	2.62		1
	Andesitic lava / volcaniclastics		2.64		2.65			5
Cretaceous - Tertiary	Granodiorite		2.51		2.51			1
	Diorite porphyry		2.67		2.68			2
	Diorite		2.80		2.80			1
	Quartz porphyry		2.50		2.50			4
	Quartz diorite		2.65		2.65			7

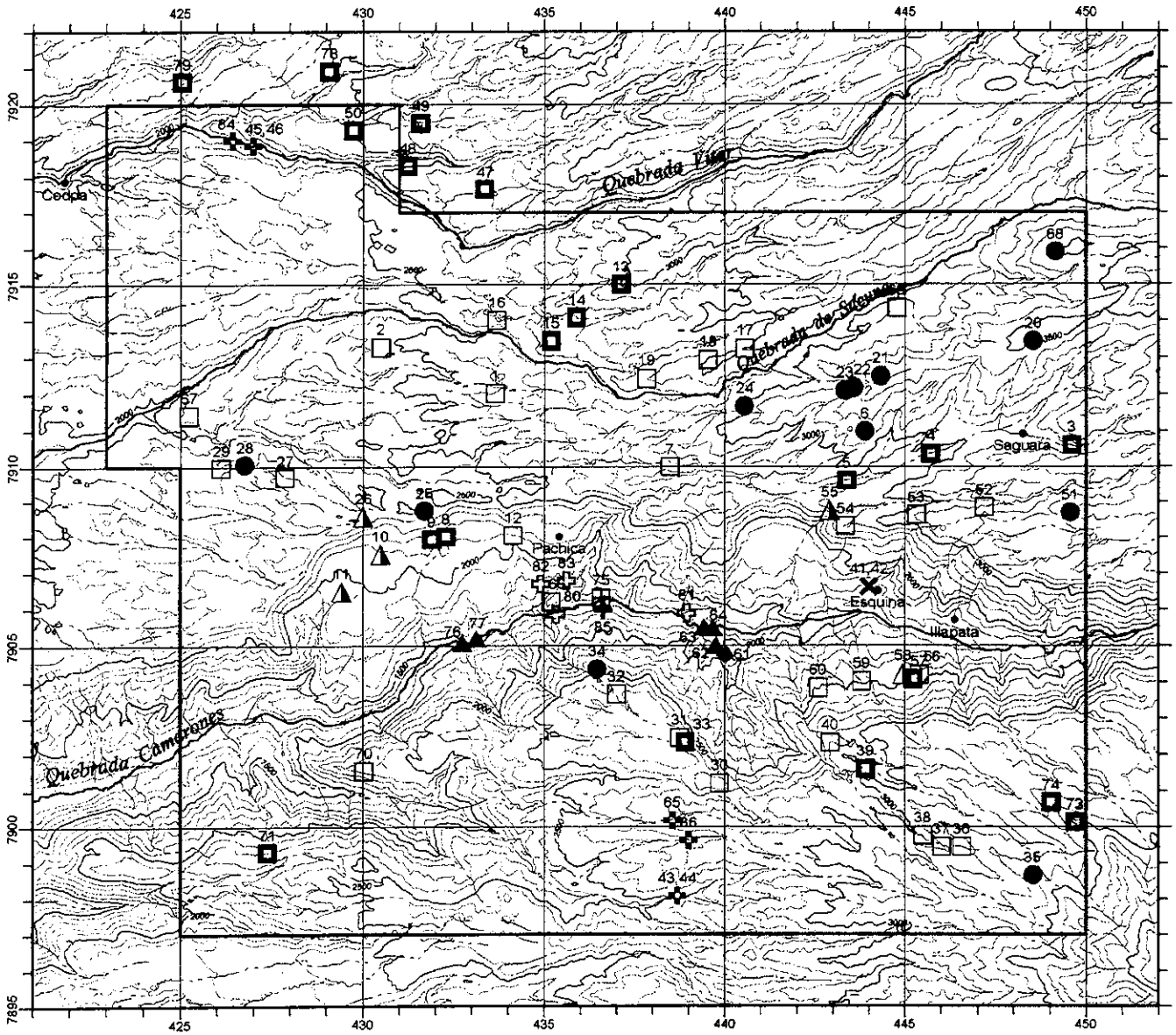

LEGEND

[Quaternary]

- Basalt
- Agglomerate

[Tertiary(Neogene)]

- Ignimbrite(Pumice tuff/ weakly welded tuff)
- Ignimbrite(Highly welded tuff)

[Cretaceous - Early Tertiary]

- Rhyolitic volcaniclastics
- Andesitic lava/ volcaniclastics

[Cretaceous - Tertiary]

- Granodiorite
- Diorite porphyry
- Diorite
- Quartz porphyry
- Quartz diorite

Fig. 2-2-3
Location of Rock Sample

the other hand, the difference between the natural dry density and the wet density is almost nil for high-density rocks and thus the effective porosity is very small.

The density of the rock samples is a basic data for determining the correction density in the terrain correction and Bouguer correction. Average density of the surface formations is important for determining the correction density. Ignimbrite is widely distributed in the Camarones district, and this rock has a wide density distribution from low-density pumiceous tuff to relatively high-density welded tuff. In such cases the actual density and simple average density may differ largely, and the average density must be calculated with consideration of the density distribution ratio. Considering the distribution ratio of [pumiceous tuff/lowly welded tuff] and [highly welded tuff] (inferred to be 2:8~1:9), the average natural dry density becomes 2.23~2.28g/cm^3 and the average wet density 2.32~2.35g/cm^3. The dry or wet conditions of the subsurface zones of the Camarones district is not exactly known, but by adopting correction density of 2.23~2.35/cm^3, reasonable results should be obtained.

2-1-2 Data processing

(1) Calculation of gravity values

In order to calculate the gravity values from the gravity meter readings, "milligal conversion", "tidal correction", "instrument height correction" and "drift correction" were carried out.

a) Milligal conversion

This process converts the dial readings to milligal value. In the case of LaCoste gravimeters, the scale constant slightly changes with the stretching of the spring. Therefore, this conversion is carried out using the milligal constant(K) and scale constant(κ) designated for every 100 units of the reading value. The basic formula for the conversion is as follows.

$$Vr = K + (R - R_0) \times \kappa \qquad (2\text{-}1)$$

Vr : Measured value in milligal

R : Gravity meter reading

R_0 : Under 100 omitted from R

b) Tidal correction

The observed gravity values vary periodically within the range of 0.2 mgal because of the following two factors. The correction for these variations is the tidal correction.

1) Periodic variation by tidal force.

2) Deformation of the earth by the tidal force (earth tide).

Tidal force is expressed by formula (2-2).

$$U=(3/2)GM(a/r^3)\{3(\sin^2\delta-(1/3))(\sin^2\phi-(1/3))+\sin 2\delta\cdot\sin 2\phi\cdot\cos\theta+\cos^2\delta\cdot\cos^2\phi\cdot\cos 2\theta\} \quad (2\text{-}2)$$

U: Tidal force of celestial body

G: Gravitational constant

M: Mass of celestial body (sun, moon etc.)

a : Distance from the center of the earth to the station (earth's radius)

ϕ : Latitude of the station

r : Distance between the earth and the celestial body

δ : Declination of the celestial body (angle from the equator)

θ : Hour angle of the celestial body (angle between terrestrial and celestial meridian plane)

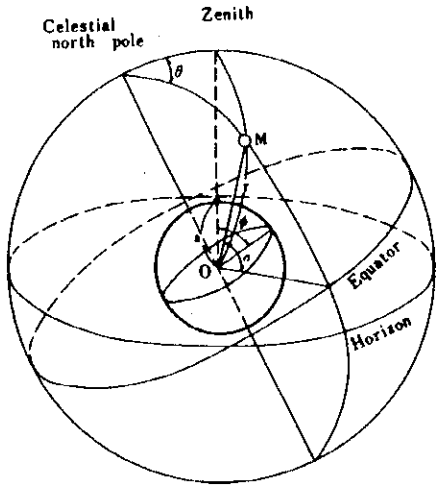

Tidal correction parameters

The tidal force of the sun and moon is overwhelmingly greater than that of other celestial bodies. Therefore, the correction for these two bodies will suffice for gravity survey.
The gravity variation caused by earth tide has the same sense as that by the tidal force and the rate of change differs somewhat by the elasticity of the rocks of the area, but it is in the order of 20 % of that caused by tidal force. Therefore, in normal tidal correction, the tidal force by the sun and moon is multiplied by 1.20, which is called the tidal constant.

c) Instrument height correction

This correction is made in order to compensate for the difference of the height for leveling and gravity measurements. The correction is done by using the vertical gradient of normal gravity on the surface of the ellipsoid of revolution (=0.3086 mgal/m) on formula (2-3).

$$Vhi \fallingdotseq (2\gamma_0/R)hi \fallingdotseq 0.3086\ hi \quad (2\text{-}3)$$

Vhi : Instrument height correction

γ_0 : Normal gravity

R : Distance from the earth's center to the station

hi : Height from the leveled point on the earth's surface to the top of the gravity meter

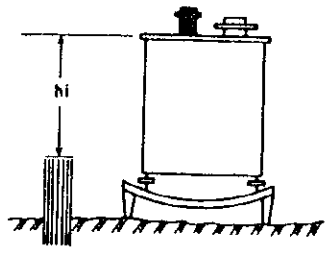

Instrument height

d) Drift correction

The drift is the variation of reading values of the gravimeter caused by the stretching of the spring. The value of the drift is roughly proportional to the lapse of time. The correction for this drift is done by time proportional allotment of the closed error to each station. The variation of readings is caused not only by drift, but also by the changes of air temperature, atmospheric pressure, mechanical shock and etc. during transportation. In practice, this process corrects also these changes.

e) Calculation of gravity values

All corrections for measured gravity values are expressed by formula (2-4).

$$Vc = Vr + Vt + Vhi + Vd \qquad (2\text{-}4)$$

Vc : Corrected gravity value

Vt : Tidal correction value

Vd : Drift correction value

The corrected gravity value Vc shows the relative value of gravity and not the absolute value of gravity. The gravity value of each station is calculated by obtaining the difference of the corrected gravity values between the station and the base station and then adding this difference to the gravity value of the base station. The gravity value of the base station is obtained by the measurement between the base station and the reference station where the gravity value is known.

(2) Gravity reduction

The process of calculating the Bouguer anomaly value is called the gravity reduction and it consists of "latitude correction", "terrain correction", "atmospheric correction", "free air correction" and "Bouguer correction".

a) Latitude correction

Subtracting "Normal Gravity" of the earth from the gravity value does this correction. Normal Gravity is given as a function of the latitude as shown in formula (2-5).

$$\gamma_0 = (a\gamma_E \cos^2\phi + b\gamma_P \sin^2\phi)/(a^2\cos^2\phi + b^2\sin^2\phi)^{1/2} \quad (2\text{-}5)$$

a: Equatorial radius of the ellipsoid of revolution(6,378.160km)

b: Polar radius of the ellipsoid of revolution(6,356.775km)

γ_E: Equatorial normal gravity of the ellipsoid of revolution(978.031 85 gal)

γ_P: Polar normal gravity of the ellipsoid of revolution(983.217 73 gal)

However, for practical gravity prospecting, the following approximation is used.

$$\gamma_0 = 978031.85(1 + 0.005278895 \sin^2\phi + 0.000023462 \sin^4\phi) \text{ (mgal)} \quad (2\text{-}6)$$

b) Terrain correction

For the present survey, the range of terrain correction was set for a radius of 60 km and the area was divided into five correction zones as follows.

The topographic elevation mesh data were prepared by reading elevation in the 1/500,000 air navigation map for the Zones A, and in the 1/250,000 topographic maps for the Zones B and in the 1/50,000 topographic maps for the Zones C－D. A sketched topographic profile of 20 m radius from the station was used for the correction of Zone E.

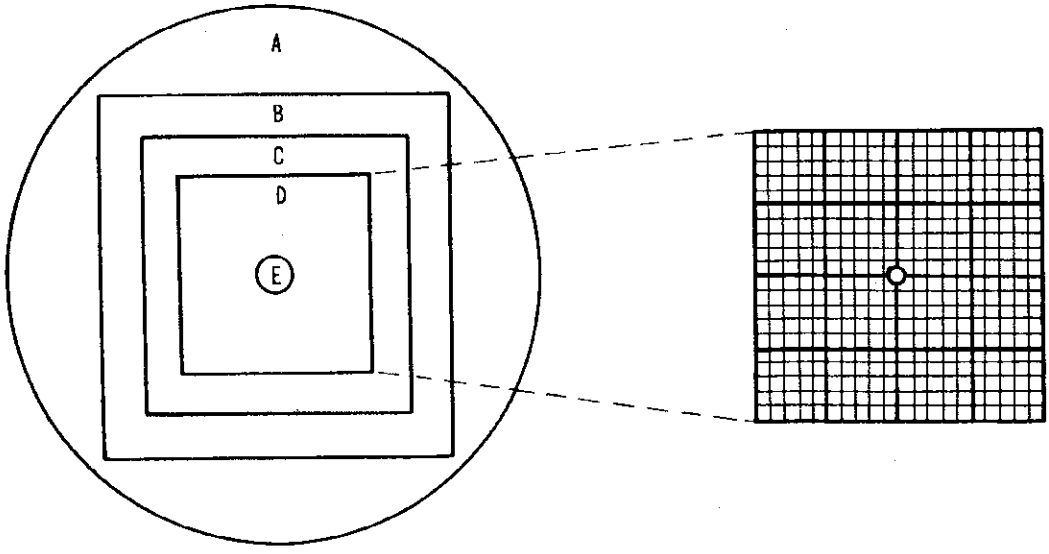

Zone	Range of correction	Mesh interval
A	60km radius	2km × 2km
B	20km × 20km	400m × 400m
C	4km × 4km	100m× 100m
D	1km × 1km	50m × 50m
E	20m radius from station	Sketched profile

Specification of terrain correction

c) Atmospheric correction

This is done in order to correct the effect of the atmosphere to gravity measurement. The atmospheric pressure will be integrated to a height of 50 km above the station using the atmospheric density distribution based on standard atmospheric model. The correction value decreases exponentially with altitude. The variation of the correction values, however, can be approximated by a linear function for altitude below 3.5 km as shown in the figure. And formula (2-7) was used for this correction.

$$\delta g_A = 0.870 - 0.0965 \times 10^{-3} H \qquad (2\text{-}7)$$

δg_A : Atmospheric correction (mgal)

H : Elevation of the station(km)

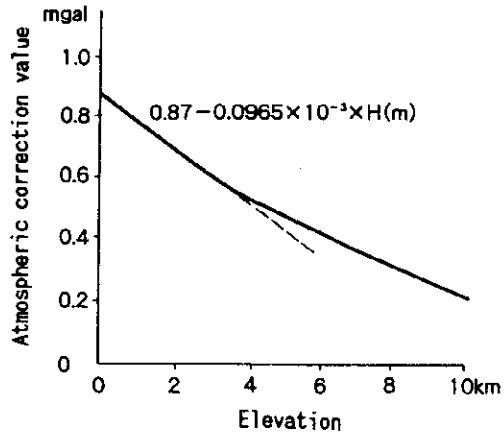

d) Free air correction

The vertical gravity gradient near the earth's surface (free air gradient) is normally -0.3086 mgal/m, and thus the gravity decreases with height. The free air correction compensates the effect of elevation for each station.

$$\delta g_F \fallingdotseq (2\gamma_0 H/R) \fallingdotseq 0.3086H \qquad (2\text{-}8)$$

δg_F : Free air correction

γ_0 : Normal gravity

R : Distance from the earth's center to the station

H : Elevation from the geoid

It is known that in areas of high elevation such as the Andes Mountains where the survey area is located, the low-density crust material is thick and that the free air gradient is smaller than -0.3086 mgal/m.

The details will be reported later, but free air gradient was examined using the measured data and the gradient of the survey area was determined to be

$$F.A.G \fallingdotseq -0.3000 \text{ mgal/m.}$$

This value was used for free air correction for this survey.

The value defined by formula (2-9) is called the free air anomaly.

$$\triangle g_F = g - \gamma_0 + \Sigma \delta g_T + F.A.G \times H \qquad (2\text{-}9)$$

$\triangle g_F$: Free air anomaly

g : Gravity value

$\Sigma \delta g_T$: Terrain correction value

e) Bouguer correction

The difference of the gravity values measured at different elevations corresponds to the attraction of the material (rocks) which exists between the elevations of the stations. Bouguer correction eliminates this difference by setting a datum plane and eliminating material between the datum and a parallel plane passing through each station. Usually geoid is used as the datum. A homogeneous circular slab, which exists between the geoid and a parallel plane including the station, is assumed for the correction formula (2-10). The radius of this slab is set at 60 km, the same as the range of terrain correction.

$$\delta g_B = -2\pi G \rho \{A + H - (A^2 + H^2)^{1/2}\}$$
$$\fallingdotseq -0.0419 \rho \{A + H - (A^2 + H^2)^{1/2}\} \qquad (2\text{-}10)$$

δg_B: Bouguer correction value

G : Gravitational constant

ρ : Density(average rock density between the geoid and earth's surface)

A : Circular slab radius (=60km)

H : Station elevation

f) Bouguer anomaly values

The values obtained by correcting the gravity values for latitude, terrain, atmosphere, free air and Bouguer are called the Bouguer anomalies and are expressed by formula (2-11).

$$\Delta g_B = g \cdot \gamma_0 + \Sigma \delta g_T + 0.870 \cdot 0.0965 \times 10^{-3} H + 0.3040 H \cdot 0.0419 \rho \{A + H \cdot (A^2 + H^2)^{1/2}\} \quad (2\text{-}11)$$

Δg_B: Bouguer anomaly value

The Bouguer anomaly is defined at the earth's surface and the value varies by the density used for the Bouguer and terrain corrections. Thus the Bouguer anomaly contains information not only on the density distribution below the geoid but also the difference of the real and the assumed density used in correction for the rocks between the geoid and the surface of the earth.

Tables of relevant data regarding this gravity survey are attached in the Appendices. These data include; location (coordinates and elevation), gravity value, normal gravity values and terrain correction values at each station, and Bouguer anomalies for ten different assumed density.

2-1-3 Analytical methods

(1) Surface fit analysis

"Surface" is a very long-wavelength gravity anomaly caused by deep subsurface structure and is also called gravity trend. Surface fit analysis is to approximate the regional gravity trend to low-order surface (multinomial formula regarding x, y). It is calculating the coefficients of the following multinomial formulas by using the Bouguer anomaly values $\Delta g(x, y)$ of grid point (x, y) by least square method.

・First order surface

$$\Delta g_1(x, y) = a_0 + a_1 x + a_2 y \quad (2\text{-}12)$$

・N-th order surface

$$\Delta g_n(x, y) = a_0 + a_1 x + a_2 y + a_3 x^2 + \cdots\cdots + \cdots + a_{m-1} x y^{n-1} + a_m y^n \quad (2\text{-}13)$$

here $m=n(n+3)/2$

Surface residual gravity is the value obtained by subtracting surface (regional trend) from the Bouguer anomaly, and this reflects the relatively shallow subsurface structure.

(2) Two-dimensional analysis

The purpose of two-dimensional gravity analysis is to construct a two-dimensional model of the subsurface structure, which would result in gravity anomalies approximating most closely those measured in the area. The gravity anomalies of the model are calculated by

the following Talwani et al.(1959) formula.

$$g = 2G\Delta\rho\,\Sigma Z_i \qquad (2\text{-}14)$$

g : Calculated gravity anomaly

G : Gravitational constant

$\Delta\rho$: Density contrast($\rho_2 - \rho_1$)

where

$$Z_i = A_i \sin\phi_i \cdot \cos\phi_i\{\theta_i \cdot \theta_{i+1} + \tan\phi_i \log B\} \qquad (2\text{-}15)$$

$$B = \{\cos\theta_i(\tan\theta_i - \tan\phi_i)\}/\{\cos\theta_{i+1}(\tan\theta_{i+1} - \tan\phi_i)\}$$

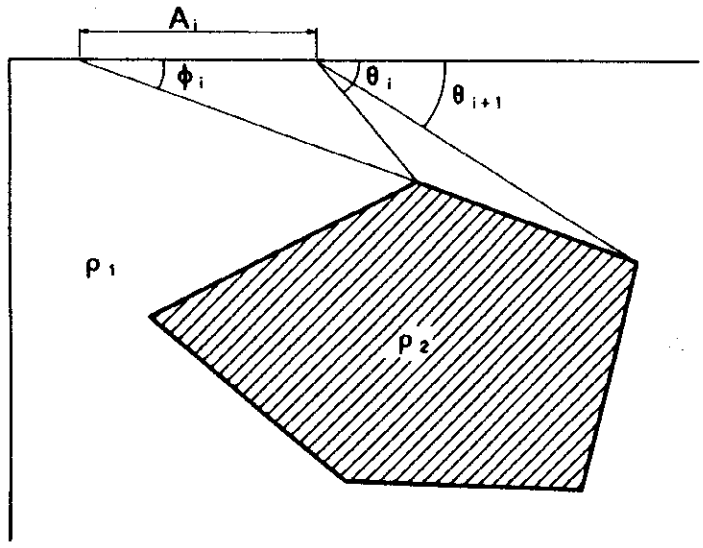

Schematic two-dimensional analysis by Talwani's method

When the geologic structure can be approximated by two layered density model, inversion method; designating a density contrast and a control depth, and then gradually altering the shape of the density boundary thus approximating the calculated values closer to the measured values can obtain unique solution.

(3) Three-dimensional analysis

Combination of prism models are assumed as shown in the figure, and the combination of the prism models, which would cause gravity anomaly approximating the measured Bouguer anomaly, is pursued by repeated calculation comparing the gravity anomaly from such models and the measured Bouguer anomaly. The vertical gravity component on surface point O by each prism is calculated by the following formula.

$$g=G\Delta\rho\,[x\ln(y+R)+y\ln(x+R)-z\tan^{-1}(xy/zR)]\Big|_{x=x-S/2,\ y=y-S/2,\ z=D}^{x=x+S/2,\ y=y+S/2,\ z=D+H} \qquad (2\text{-}16)$$

S: Width of prism

R: Lateral distance from Point O to the center of prism

D: Depth from the surface to the upper surface of the prism

H: Height of the prism from the datum plane

Gravity anomaly at Point O is given by the total sum of the g of all prisms.

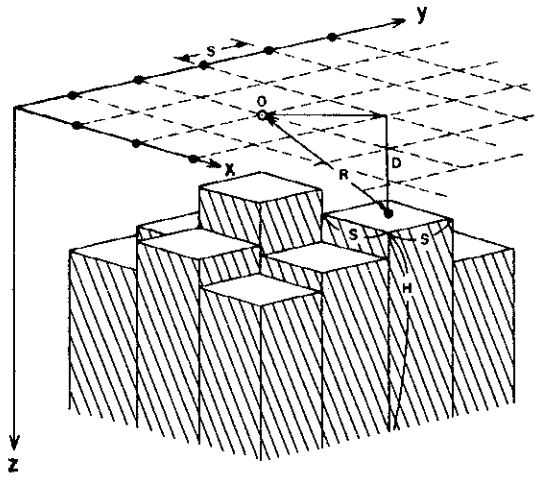

Schematic three-dimensional analysis by prism model

2 - 2 Results of the Survey

2-2-1 Free air gradient and Bouguer density

Free air gradient and Bouguer density were studied by using "Nettleton profile". This method is as follows. Several Bouguer anomaly profiles with different correction density (Bouguer density) are prepared along a profile with large topographic relief, and the correlation between the topography and each Bouguer anomaly profile is compared and examined. The correction density is selected by discriminating the Bouguer anomaly profile with the least correlation with topography.

Nettleton profiles for three sections, A－B, C－D, and E－F of Figure 2-2-4, were prepared.

These profiles are laid out in Figures 2-2-5 ~ 2-2-7. In each figure, Bouguer anomaly profiles of three free air gradients, namely -0.3086 mgal/m, -0.3040 mgal/m, and -0.3000 mgal/m are shown from the top downward, and topography is shown in the bottom. Bouguer anomaly profiles with seven correction densities, 2.00, 2.20, 2.30, 2.40, 2.50, 2.60, 2.67 g/cm^3 were prepared. Appropriate density (correction density for Bouguer anomaly with least correlation with topography) was determined individually for valleys and ridges where the correlation between topography and Bouguer anomaly is clearly observed. These density values are shown digitally in the figure. The Bouguer anomaly profile judged to have the least correlation with topography is shown in bold line.

The appropriate correction density values obtained from the examination of Nettleton profiles are listed below.

Free air gradient (mgal/m)	Appropriate correction density (g/cm^3)		
	A－B section	C－D section	E－F section
-0.3086	2.40～2.50	2.40～2.50	2.40～2.50
-0.3040	2.30～2.40	2.30～2.40	2.30～2.40
-0.3000	2.20～2.30	2.20～2.30	2.20～2.30

It is seen from this table that the appropriate correction density tends to decrease with the free air gradient values. Also the appropriate correction density values are the same in all profiles for free air gradients with the same value.

The average density of the ignimbrites widely distributed in the Camarones district is inferred to lie with the range of 2.23 ~ 2.35 g/cm^3 in 2-1-1-(3). This average density of ignimbrite would correspond to free air gradient of –0.3020 mgal/m, which is between –0.3040 mgal/m and –0.3000 mgal/m.

Also data regarding appropriate correction density were obtained by two-dimensional two-layered structure analysis. This analysis was carried out assuming a two-layered structure consisting of the basement (average density 2.65g/cm^3) and the overlying formations. It was clarified that the most appropriate results were obtained by assuming the density contrast between the basement and overlying formations to be 0.40 g/cm^3. This density contrast shows that the average density of the overlying formations is 2.25g/cm^3. As the overlying layers consist mostly of surface material, it is considered that this value would be best for use as correction density for gravity correction. The density value of 2.25g/cm^3 is within the average density value of ignimbrite inferred from the density of rock samples, and

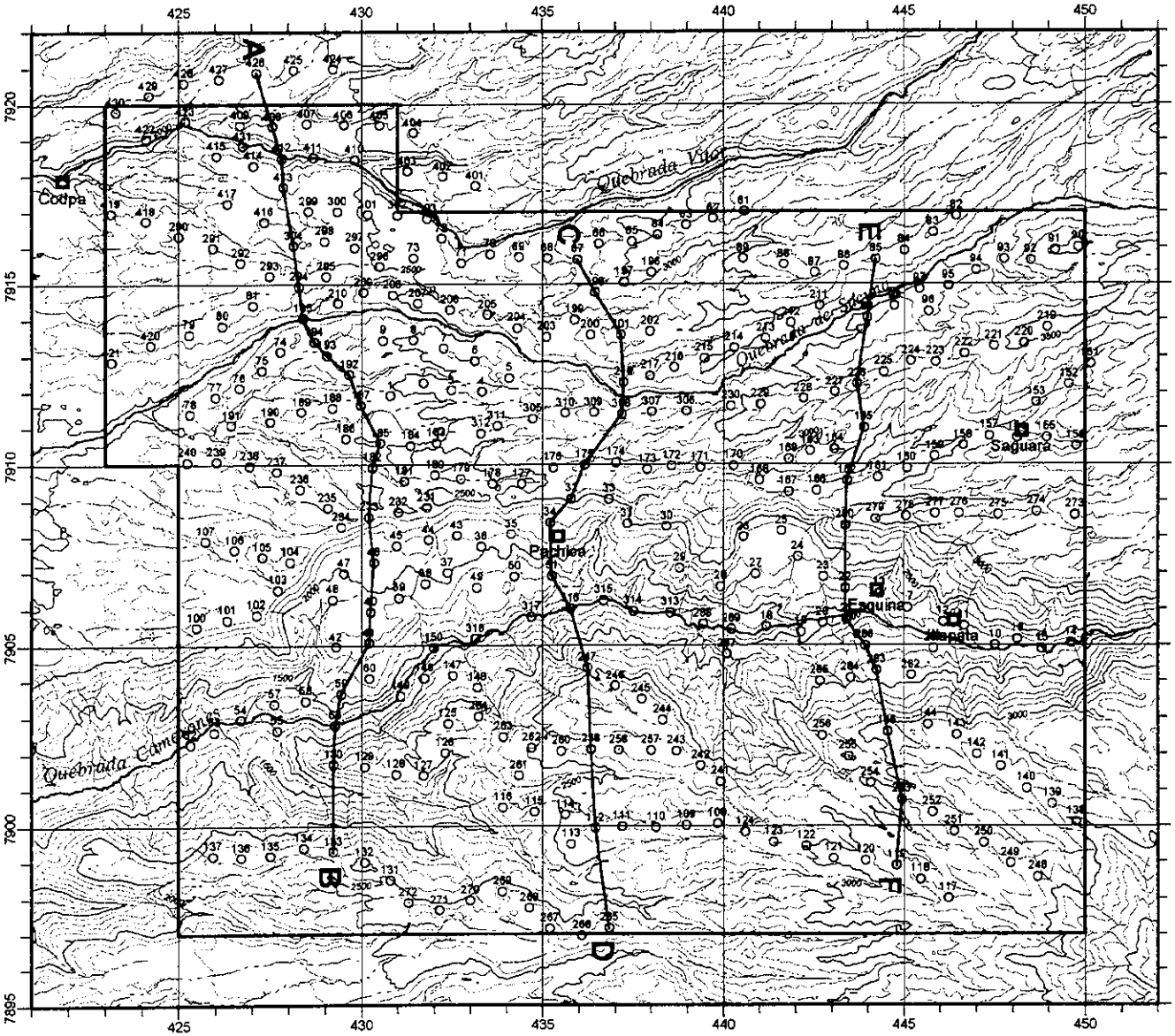

LEGEND

○ Gravity Station

Nettleton Profile Line

Fig. 2-2-4
Location of Nettleton Profile

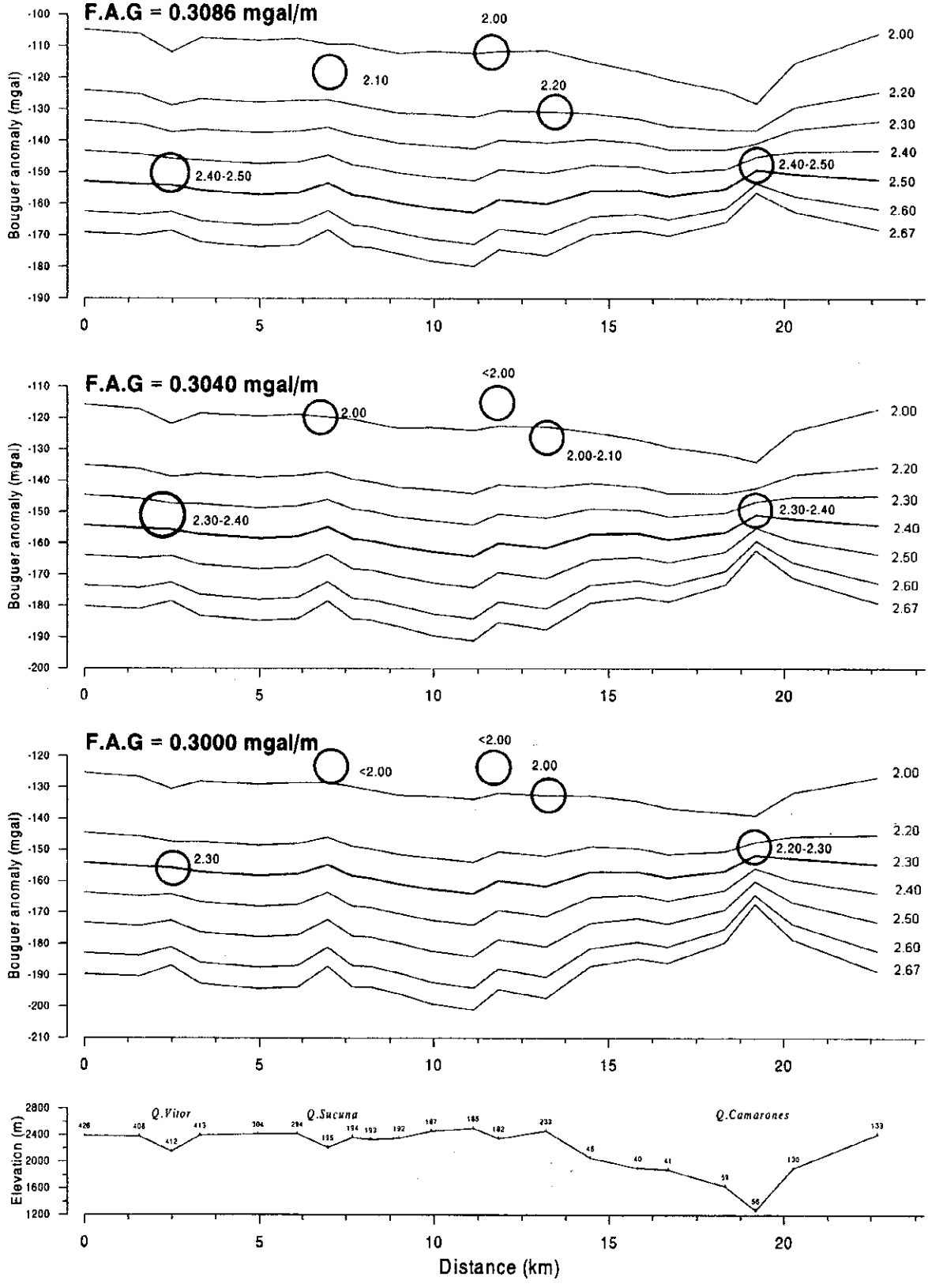

Fig. 2-2-5 Nettleton Profile of Section A-B

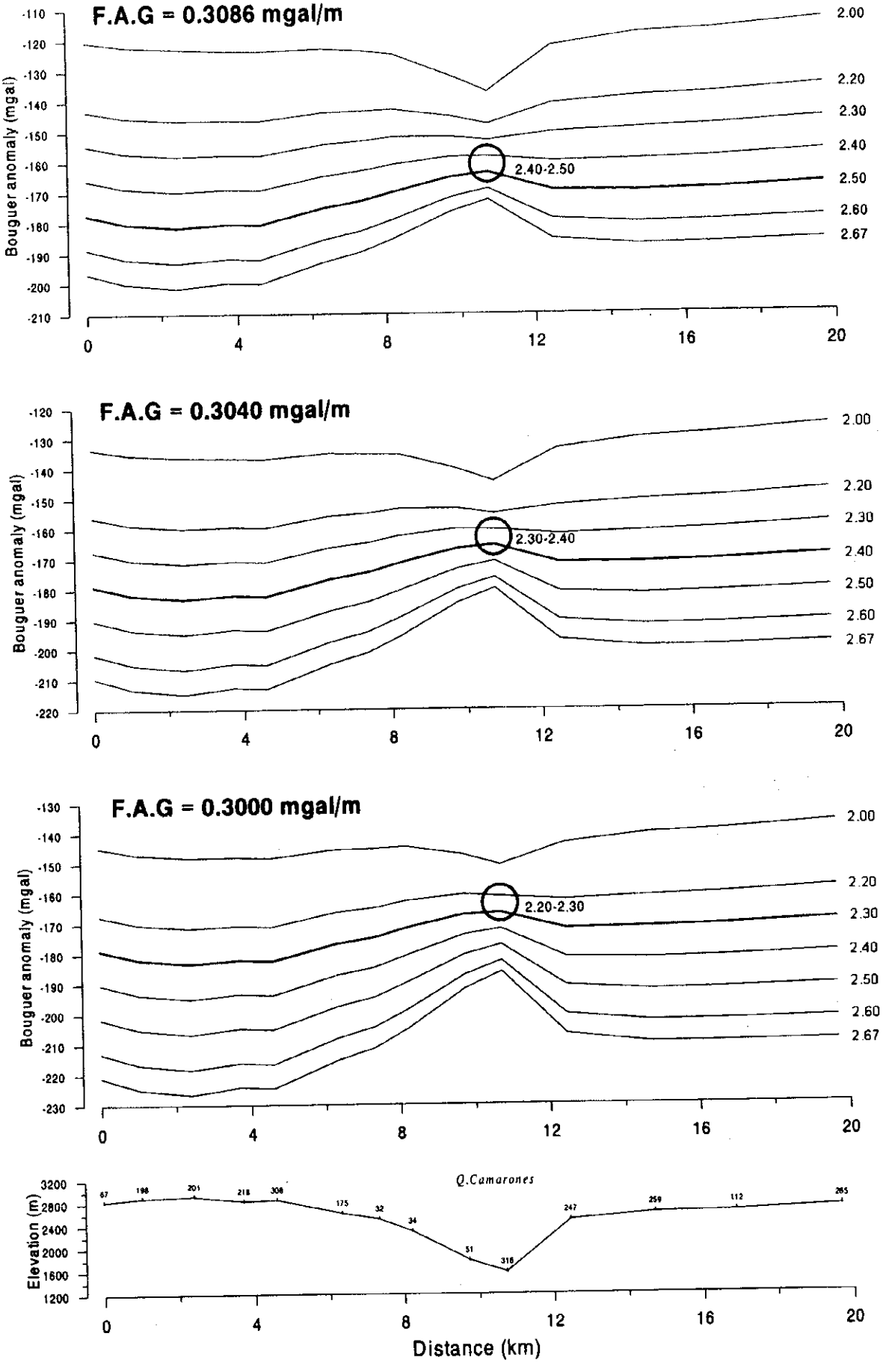

Fig. 2-2-6 Nettleton Profile of Section C-D

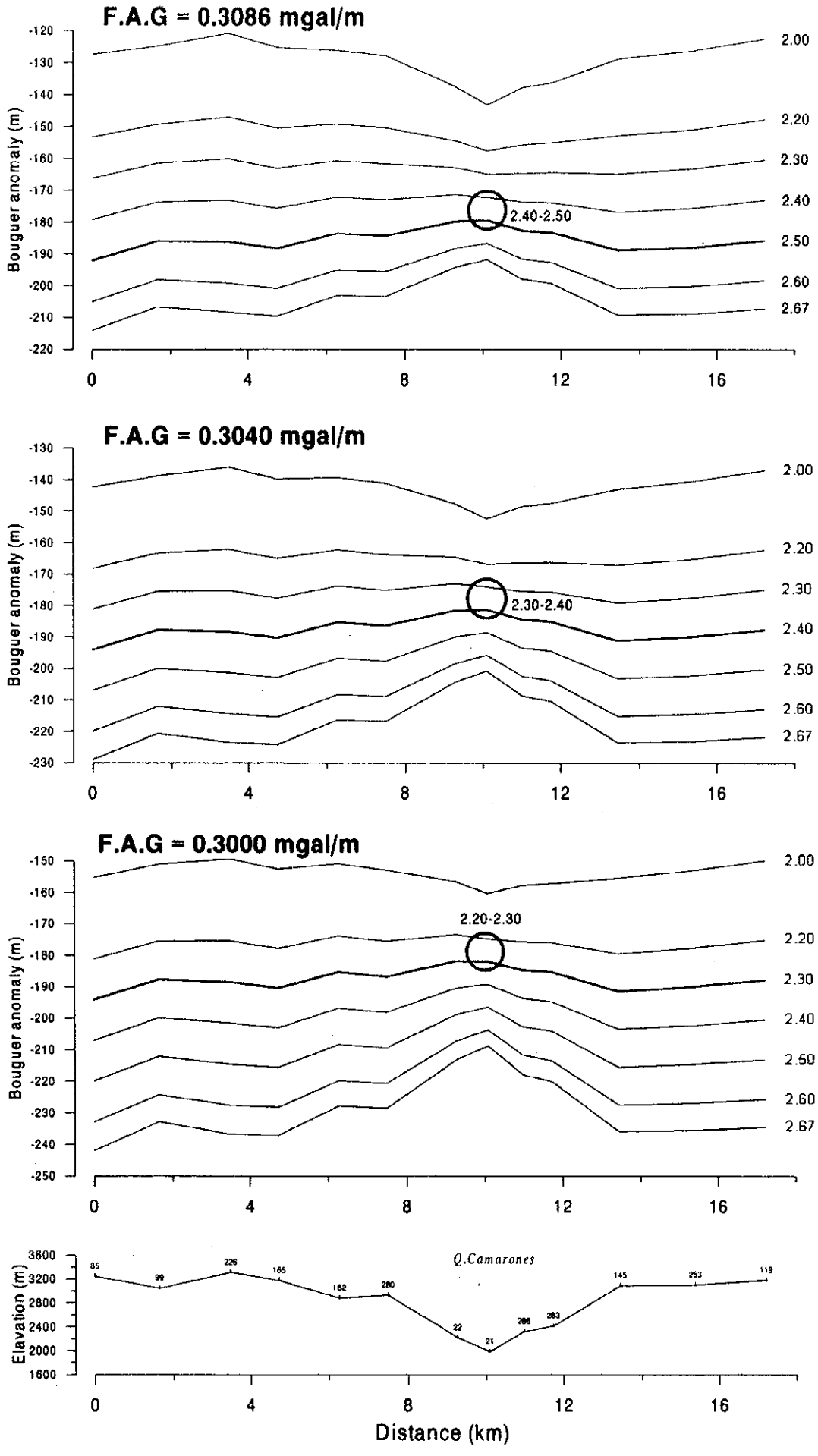

Fig. 2-2-7 Nettleton Profile of Section E-F

thus does not contradict the results of density measurements.

Since 2.25 g/cm^3 is the most appropriate value, free air gradient of –0.3000 mgal/m, which corresponds to appropriate correction density of 2.20~2.30 g/cm^3, is considered to be appropriate. Thus the final Bouguer anomaly map was prepared with free air gradient –0.3000 mgal/m and correction density ρ =2.25 g/cm^3.

2-2-2 Gravity anomaly maps

In this section, the location will be designated mainly streams, namely Quebrada Camarones, Quebrada Sucuna, and Quebrada Vitor. And upstream, middle stream, and downstream will be used to denote the relative location in each map. In other words, the maps will be divided into three sections in the east-west direction, and eastern part will be upstream, the central part will be middle stream, and the western part will be downstream.

(1) Bouguer anomaly maps

A Bouguer anomaly map with free air gradient of -0.3000 mgal/m and correction density of ρ =2.25 g/cm^3 is shown in Figure 2-2-8. Also four other kinds of Bouguer anomaly maps based on ρ =2.00, 2.20, 2.30, and 2.50 g/cm^3 are laid out in Figure 2-2-9 in order to compare the difference of gravity distribution by correction density. All these gravity maps have been prepared by using data with grid interval of 500 m.

The following features are noted in the Bouguer anomaly maps in Figure 2-2-9 regarding the gravity features along the Quebrada Camarones where the topographic relief is high.

① In the ρ =2.00 g/cm^3 map, conspicuous low-gravity anomaly extends along the Quebrada Camarones where the elevation is low and this indicates insufficient correction. On the other hand, in the ρ =2.50 g/cm^3 map, the Quebrada Camarones is shown as a high-gravity anomaly zone, this indicates excess correction.

② In the ρ =2.20 g/cm^3 and ρ =2.30 g/cm^3 maps, no large scale anomaly reflecting the topography exists, but slight high-gravity anomaly extends eastward along the Quebrada Camarones from the west in the ρ =2.30 g/cm^3 map. This indicates that ρ =2.30 g/cm^3 is a slightly high correction density for this zone.

The five Bouguer anomaly maps shown in Figures 2-2-8 and 2-2-9 all show high Bouguer anomaly in the western side and rapidly decrease eastward. Regional crustal structure is inferred to cause such steep Bouguer anomaly inclination (gravity trend). In order to

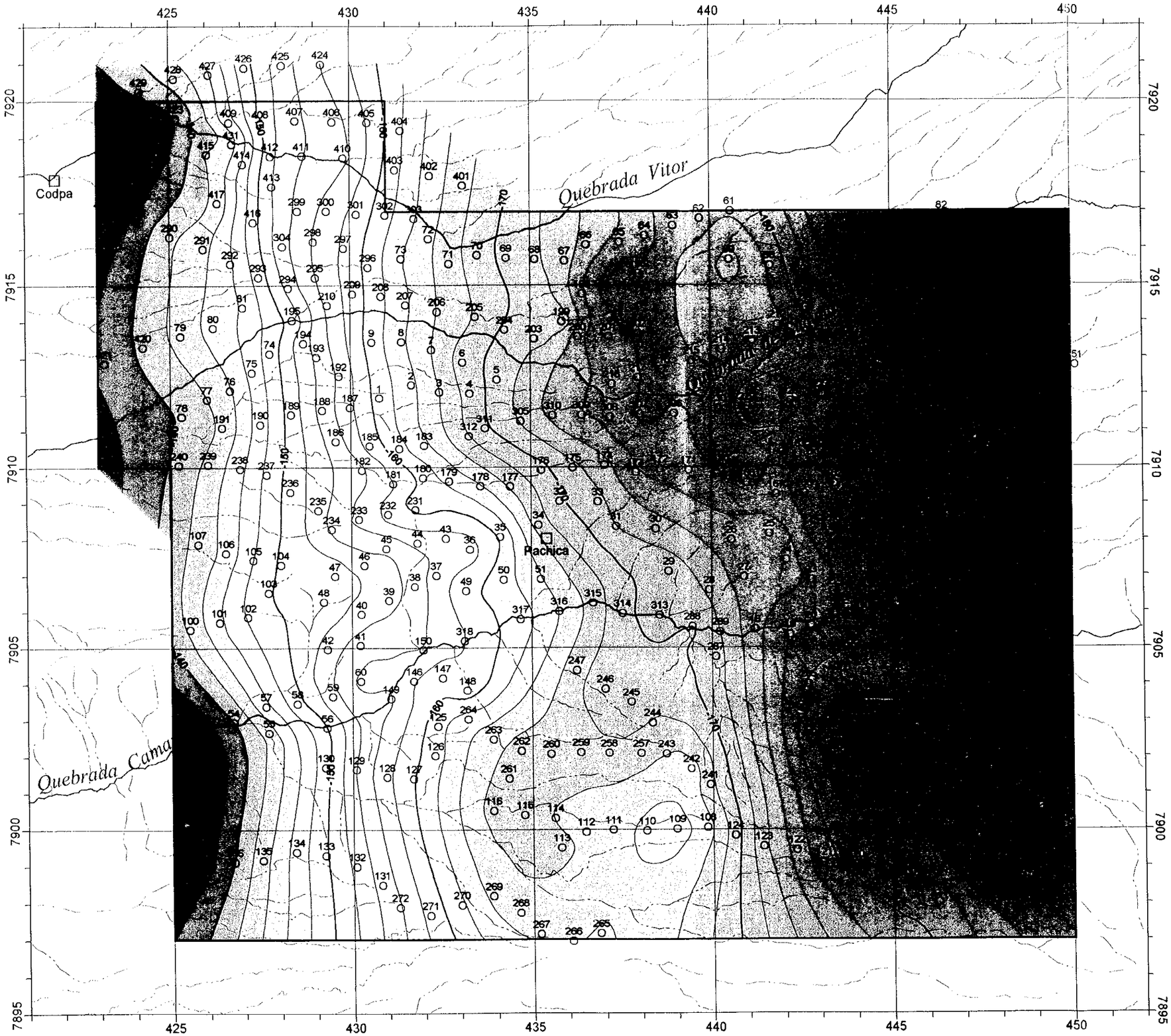

Fig. 2-2-8
Bouguer Anomaly Map
(F.A.G=-0.3000 mgal/m)
ρ =2.25 g/cm^3

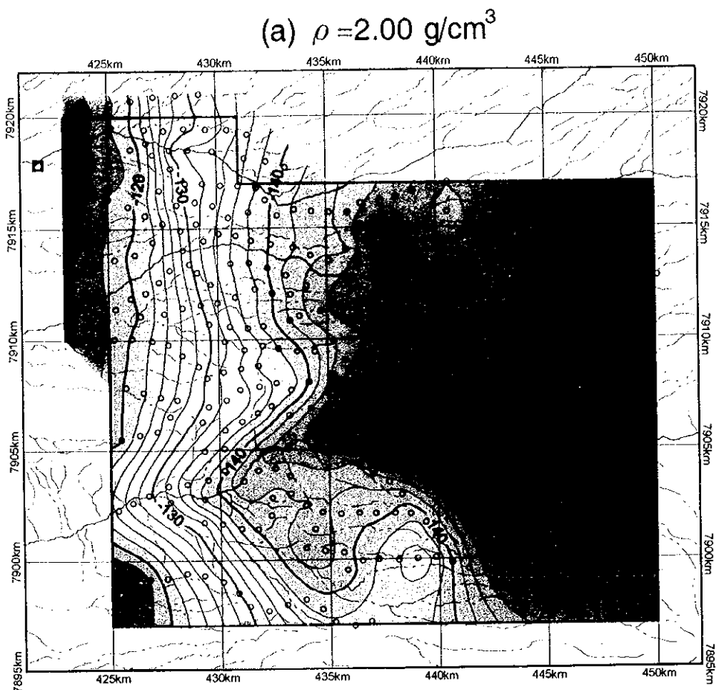

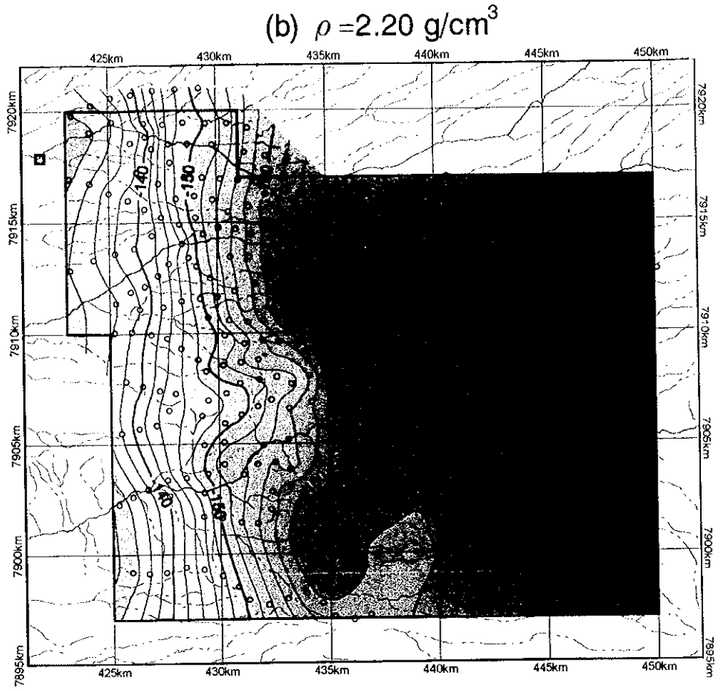

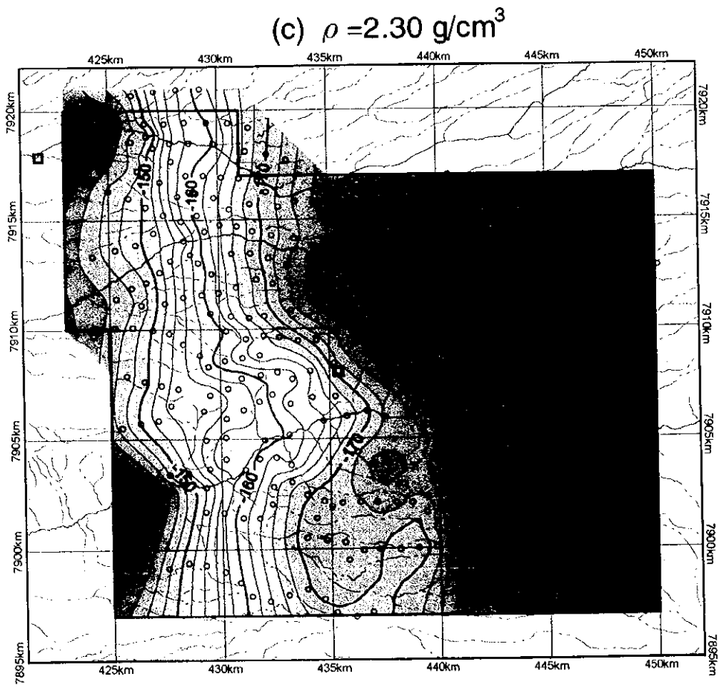

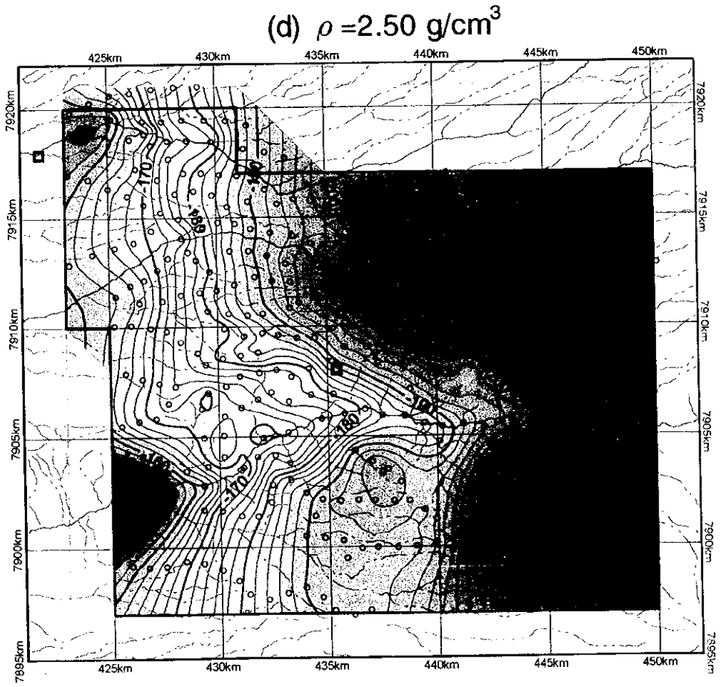

Fig. 2-2-9
Bouguer Anomaly maps
(F.A.G = -0.3000 mgal/m)

confirm this, more gravity measurements were made along a road from the survey area to the Pan American Highway about 30km west. The interval between stations was about 2km. The result of this measurement is shown in Figure 2-2-10.

It is seen from Figure 2-2-10 that the gravity trend of eastward decrease covers not only the survey area, but also the wide region and the trend has almost constant inclination. In the western slope of the Andes Mountains, where the present survey area is located, upper part of the continental crust with relatively low density becomes thicker to the east. This regional variation of crust thickness is considered to cause the regional gravity trend of this area mainly.

(2) Trend map and residual map

As mentioned in the previous section, the Bouguer anomaly distribution of the survey area incorporates the gravity trend caused by the variation of the crust thickness. Therefore, the gravity trend must be removed from the Bouguer anomaly in order to prepare a gravity anomaly map reflecting the relatively shallow subsurface structure of the survey area.

This is carried out as follows. First simply calculate the first order trend by using the 500m-interval grid data of Bouguer anomaly and prepare a first order residual map (Fig. 2-2-11(a), (b)) by deducting the calculated trend from the Bouguer anomaly. The inclination of the trend obtained from above process was not exactly in the E-W direction, but in the WSW-ENE direction. The highest anomaly value in the residual map appeared in the northwestern edge of the survey area, and not in the Quebrada Camarones zone where the basement rocks are widely distributed nor in the southernmost part of the area where existence of large-scale intrusive body is inferred. Figure 2-2-11 (b), therefore does not show gravity features harmonious with the distribution of geologic units.

The reason for the appearance of the maximum residual gravity value in the northwestern edge in the residual map (Fig. 2-2-11 (b)) is the northern component of the calculated trend, WSW-ENE, and not E-W as the geology indicates. There is a NW-SE trend in the geologic structure of the Camarones district, and thus it is possible that the northern component of the gravity trend reflects the geologic structure of the Camarones district and is not a regional component. Next the trend was re-calculated by limiting the direction of inclination to exactly E-W. The results are shown in Figure 2-2-11 (c) and (d). The residual map (d) shows the location of the maximum residual gravity value in the southernmost part of the survey area, and its gravity features are more harmonious with the

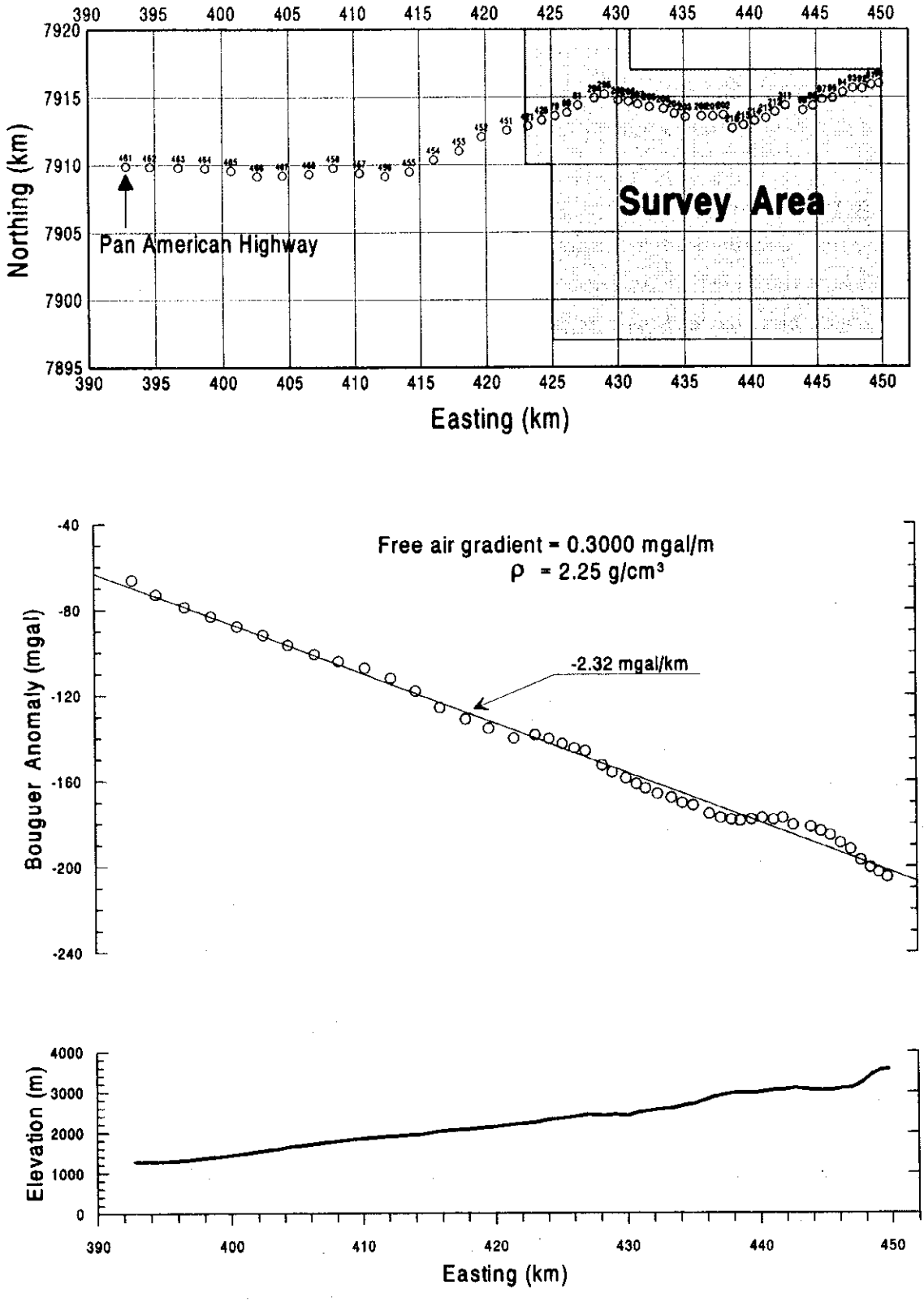

Fig. 2-2-10 Regional Gravity Trend

(a) First order trend(1)

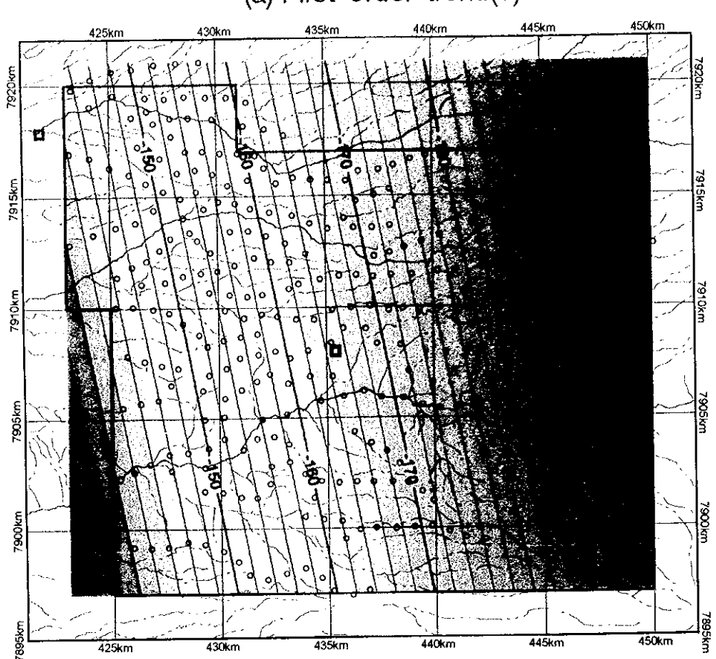

(b) First order residual(1)

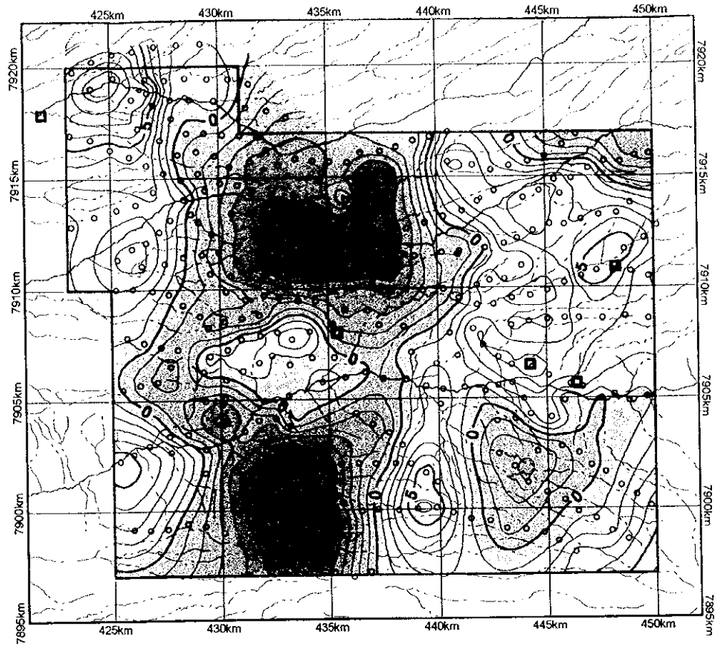

(c) First order trend(2)

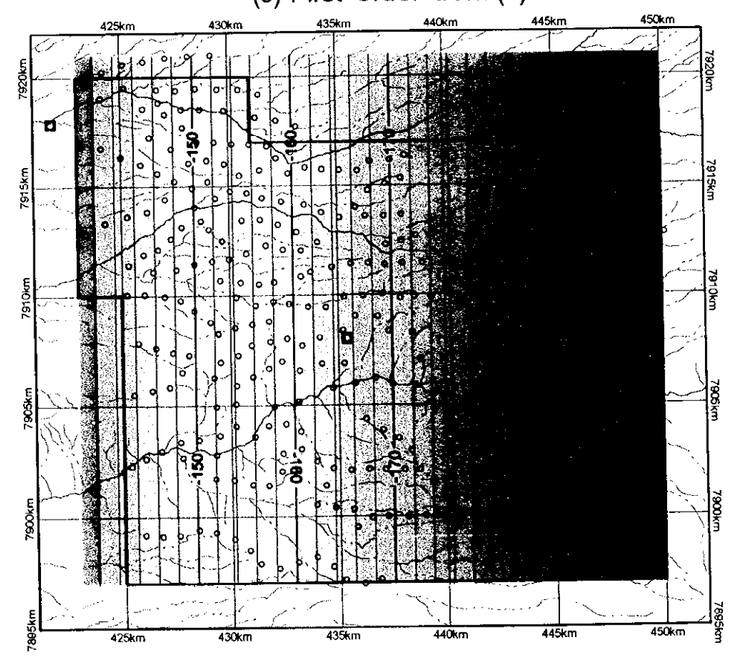

(d) First order residual(2)

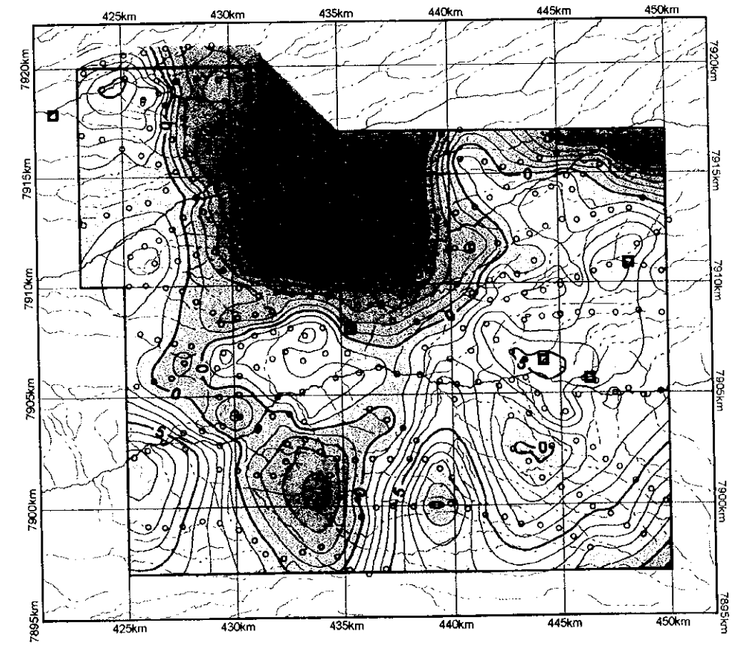

Fig. 2-2-11
Trend maps and Residual maps
(F.A.G = -0.3000 mgal/m)
(ρ =2.25 g/cm^3)

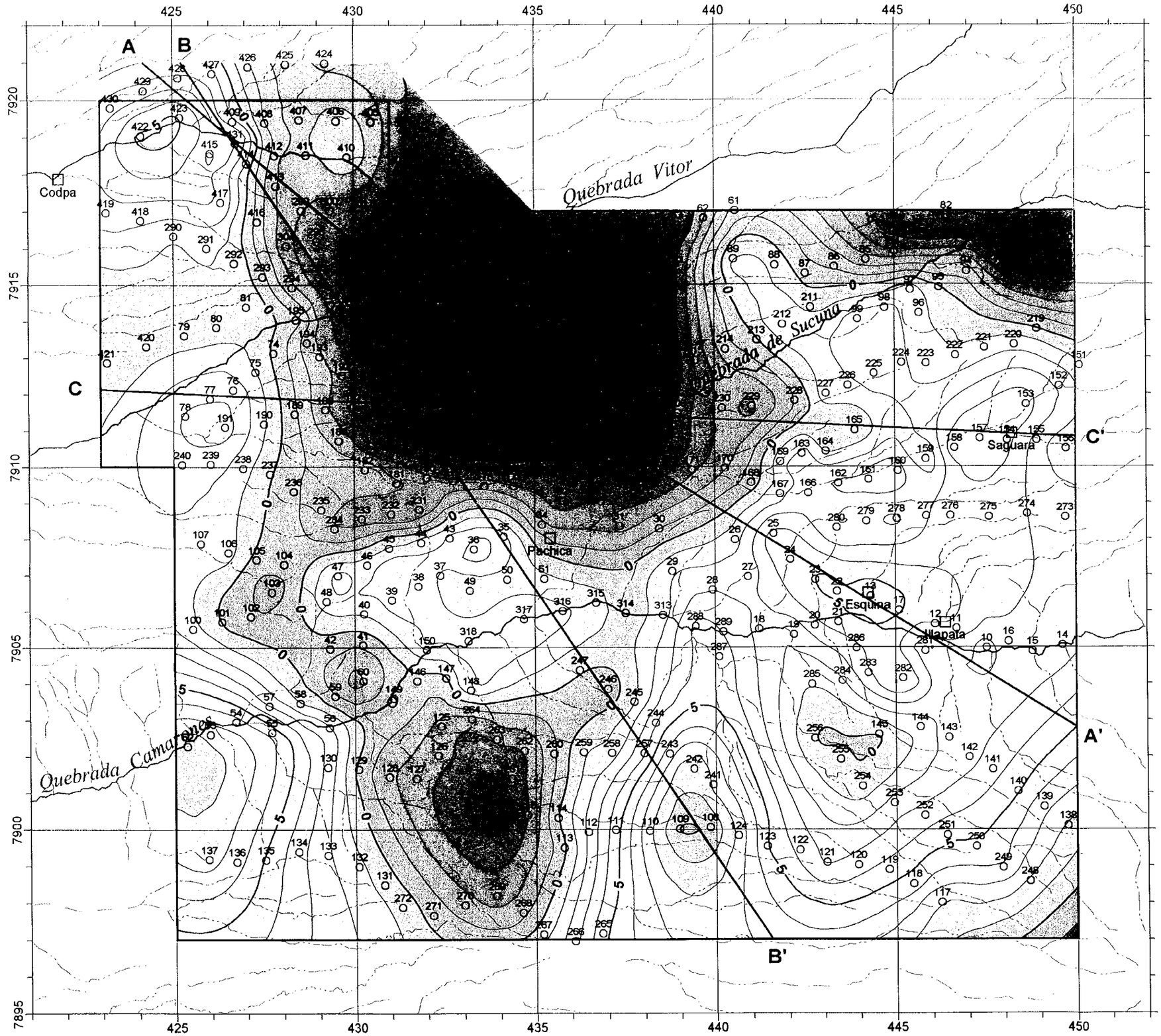

LEGEND

123 ○ Gravity station and number

—— Section of 2D analysis

16mgal
11mgal
6mgal
1mgal
-4mgal
-9mgal
-14mgal

Fig. 2-2 -12
Residual Gravity Map
(F.A.G = -0.3000 mgal/m)
ρ =2.25 g/cm^3

(a) ρ =2.20 g/cm^3

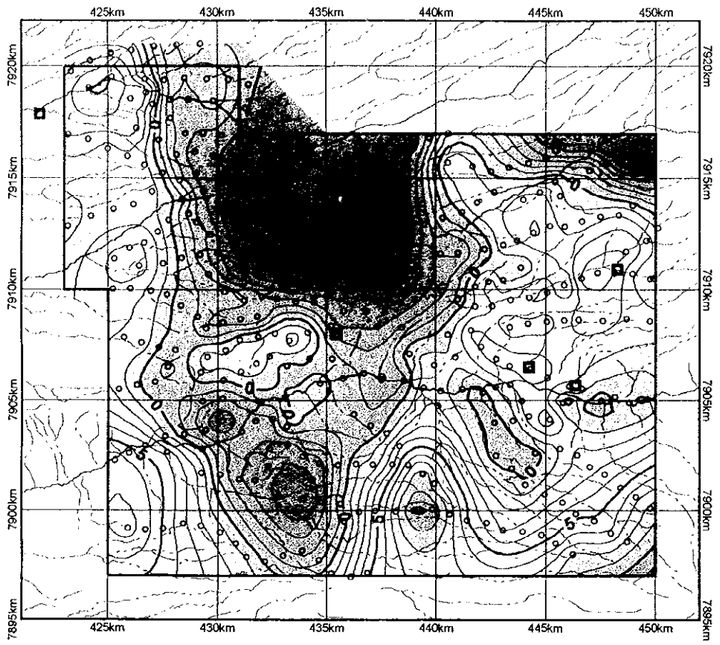

(b) ρ =2.25 g/cm^3

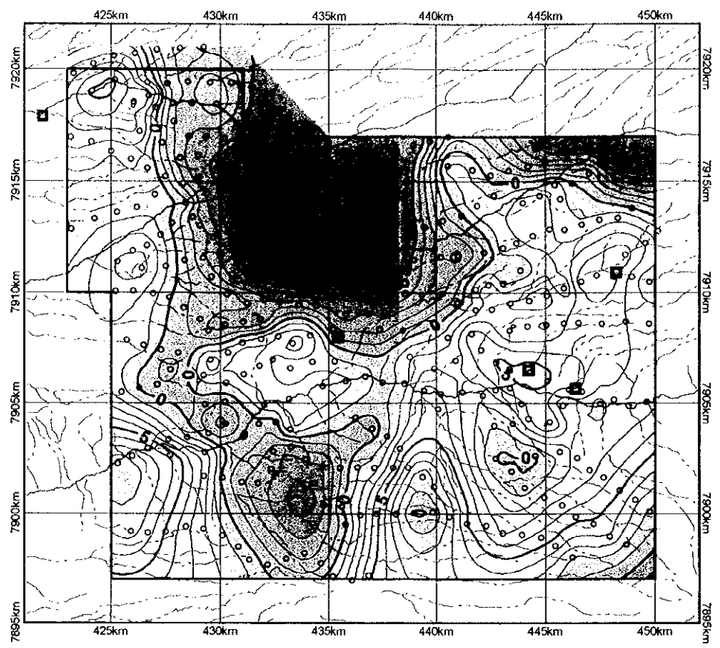

(c) ρ =2.30 g/cm^3

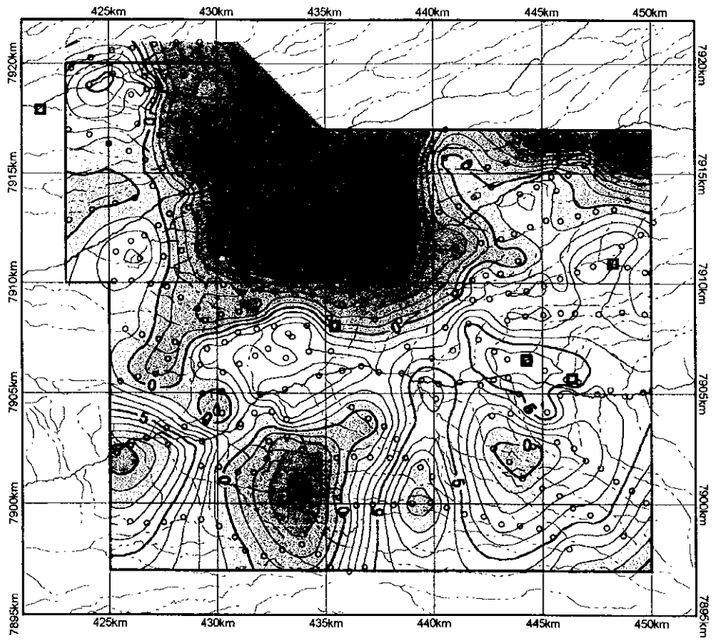

Fig. 2-2-13
Residual gravity maps
(F.A.G = -0.3000 mgal/m)

geology compared to the map (b). Therefore Figure 2-2-11 (d) was used for analysis and interpretation.

The Figure 2-2-11 (d) residual map is converted to 1:100,000 scale and shown in Figure 2-2-12. For comparison, three kinds of residual maps with ρ=2.20 g/cm^3, ρ=2.25 g/cm^3, and ρ=2.30 g/cm^3 are laid out in Figure 2-2-13. It is seen from this figure that the ρ=2.30 g/cm^3 map shows some correlation between gravity anomaly and topography along the Quebrada Camarones indicating ρ=2.30 g/cm^3 to be a little high for the correction density.

The ρ=2.25 g/cm^3 residual map of Figure 2-2-12 shows distribution of high gravity anomalies at a wide zone from the eastern part to the southeastern and southern part of the survey area, westernmost part extending along the northwest margin to the southwest margin of the survey area, and the zone from middle reaches of Quebrada Camarones in the central part to the west of Pachica. On the other hand, low gravity anomalies occur in a wide zone from middle reaches of Quebrada Vitor to the middle reaches of Quebrada Sucuna in the northern part, on the south of Quebrada Camarones in the southwest, and in the upper reaches of Quebrada Sucuna in the northeastern edge of the survey area. A low gravity anomaly occurs over an area of 5km×5km in the southeastern part but this is a local occurrence and the southeastern part of the survey area is considered to be, on the whole, a high gravity zone. The low gravity anomaly between middle Quebrada Vitor and middle Quebrada Sucuna is characterized by a relatively high gravity gradient in the eastern, southern, and western margins resulting in an anomaly zone with a clear outline.

The highest residual gravity value occurs near Station No.109 at the southernmost part of the area followed by the value near Station No.52 at the southwestern margin of the area. The lowest gravity anomaly value occurs near Station 197 in the northern part, and the second lowest value extends over an area of 3km E-W and 2km N-S on the south of the middle stream of the Quebrada Sucuna.

The basin of the Qubrada Camarones is almost all in the high gravity zone with the exception of a part of the southwestern part.

2-2-3 Gravity anomalies and aeromagnetic anomalies

Aeromagnetic map (reduction to the pole map) of the Camarones district is shown in Figure 2-2-14. The magnetic map on the left side of Figure 2-2-14 is a reduction to the pole map

before filtering, and that on the right side is a reduction to the pole map after a high-cut filtering with wavelength threshold of about 2.5 km. The magnetic maps before filtering is strongly affected by topography while the effect of topography is almost completely eliminated in the magnetic map after filtering.

Reduction to the pole map and residual gravity map are laid out in Figure 2-2-15 for examining the relation between gravity anomalies and magnetic anomalies. It is seen in Figure 2-2-15 that low gravity anomalies correspond well with high magnetic anomalies in the northern to the central part of the area while high gravity anomalies and low magnetic anomalies correspond to each other in the eastern part. Also high gravity and high magnetic anomalies coincide well at two localities in the southernmost and northwestern margin of the area, and low gravity anomalies nearly coincide with low magnetic anomalies in the southwestern to the southern part.

The above is summarized as; "high gravity - low magnetic" and "low gravity - high magnetic" correlation occurs in large-scale anomalies while "high gravity – high magnetic" and "low gravity - low magnetic" relation exists for local-scale anomalies.

2-2-4 Two-dimensional analysis

Two-dimensional analysis was carried out for three sections A−A', B−B', and C−C' of Figure 2-2-12. Analysis was done by both two-layer and multi-layer modeling and the results are shown in Figures 2-2-16~2-2-18. In these figures, measured and calculated gravity anomalies (residual gravity) values are shown in the top section, two-layer modeling results in the middle, and the multi-layer modeling results in the bottom.

The measured gravity profile is shown by red line, the calculated gravity anomaly values by different symbols for two-layer modeling (3 density contrasts) and multi-layer modeling results. Also magnetic anomaly (reduction to the pole) profile along the same section is shown by blue line for reference.

Two-layer modeling is an analytical method of examining the difference of the depth to the basement surface (or thickness of the volcanic rocks) by the following process. The subsurface density structure is divided into the upper and lower layers with the basement surface as the boundary, and then the density contrast ($\Delta \rho$) of the two layers is varied. Modeling was carried out for three density contrasts; $\Delta \rho = 0.30$, 0.40, and 0.50 g/cm^3.

(a) Non filtered

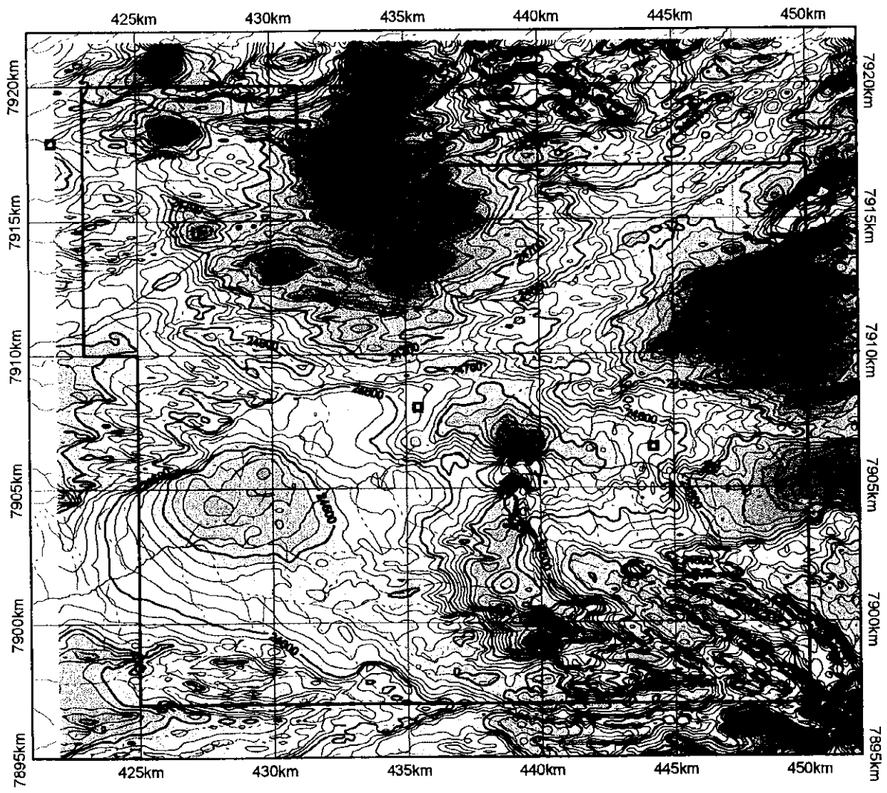

(b) High-cut filtered

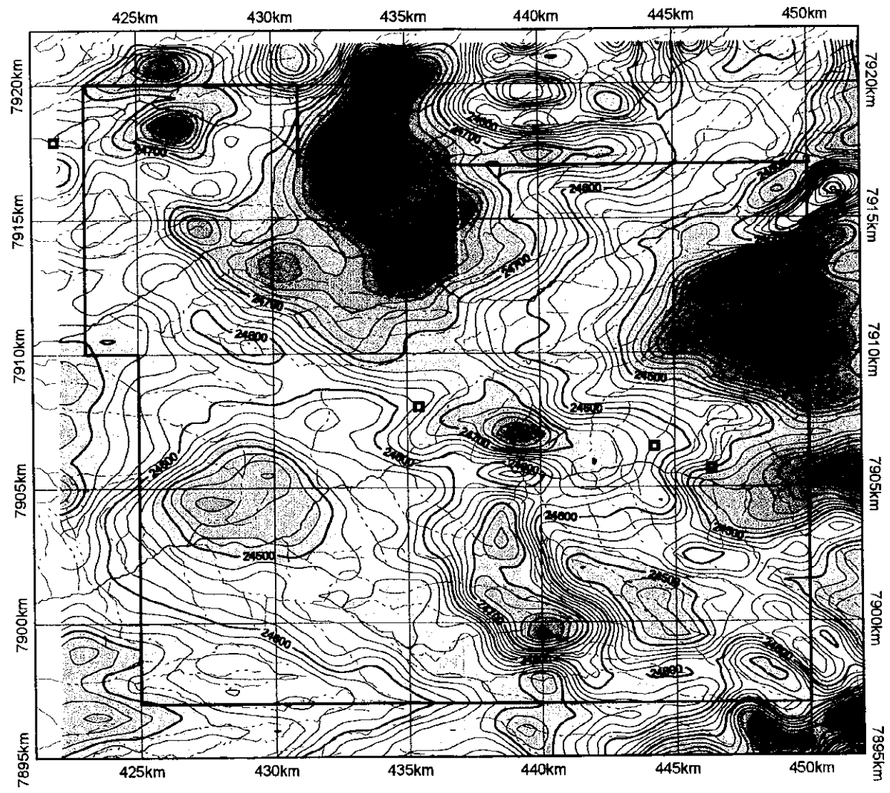

Fig. 2-2-14 Aeromagnetic Maps (Reduction to the pole)

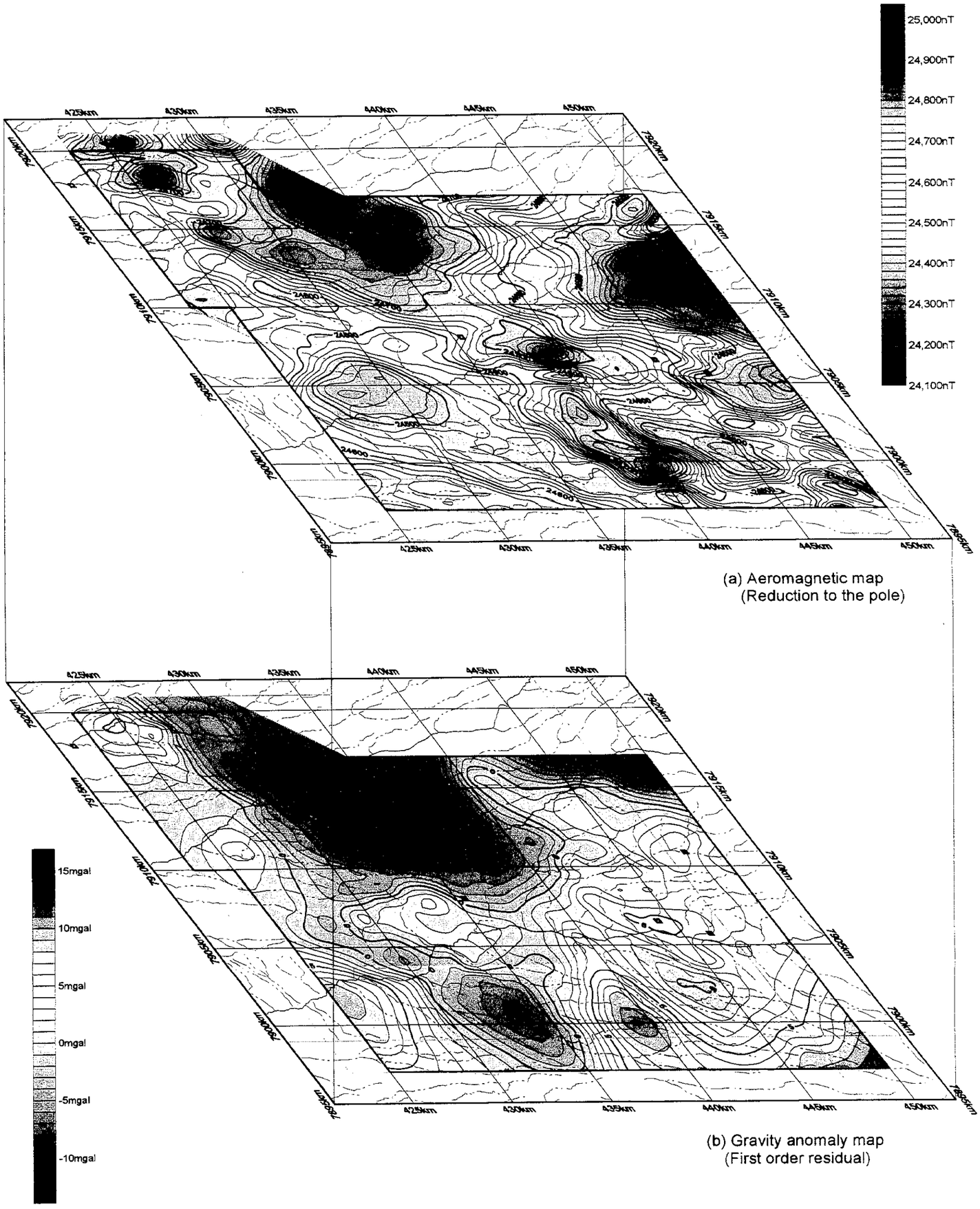

Fig. 2-2-15 Panel Diagram of Aeromagnetic Map and Gravity Map

Assuming the average density of the basement to be 2.65 g/cm^3, these three density contrasts correspond to the average densities of 2.35, 2.25, and 2.15 g/cm^3 for the upper layer

The control points for two-layer modeling were set at locations where the basement is exposed at the surface for sections A−A' and B−B'. Since the basement is not exposed along the section C−C', the calculated depth of the section A−A' at the intersection between sections C−C' and A−A' was used as the control point.

The stratigraphic division used for multi-layer modeling is as follows.

[Quaternary System]	
Conglomerate, gravel layer	2.00 g/cm^3
Agglomerate/andesite, basalt	2.25/2.60 g/cm^3
[Neogene System]	
Low-density ignimbrite (mainly pumiceous tuff)	1.85 g/cm^3
High-density ignimbrite (mainly welded tuff)	2.30 g/cm^3
Conglomerate	2.15 g/cm^3
[Basement complex]	
(Upper Cretaceous, Upper Cretaceous~Paleogene Systems, intrusive rocks)	
Rhyolitic pyroclastics, andesite lava, andesite pyroclastics	2.65 g/cm^3
Diorite porphyry	2.67 g/cm^3
Quartz diorite	2.65 g/cm^3
Quartz porphyry·granodiorite	2.55 g/cm^3

Density value of 2.25 g/cm^3 was used for Quaternary agglomerate, andesite, basalt in localities with higher occurrence of agglomerate, and 2.60 g/cm^3 for localities with higher andesite and basalt occurrence. Density data regarding conglomerate and gravel layers are lacking, and the value 2.00 g/cm^3 was determined by trial and error method seeking fair agreement of calculated and measured gravity anomaly values.

The Neogene ignimbrite was divided into two groups, low-density and high-density groups. This division is based on average density of naturally dried values. High-density ignimbrites constitute the major part of the upper layer in two-layer modeling, and 2.25 g/cm^3 was considered to be the appropriate density from the modeling results. Thus the actual density of the high-density ignimbrite is most probably lower than the average density 2.33 g/cm^3 of rock samples and the value 2.30 g/cm^3 was used. There are no density data regarding conglomerate. And since conglomerate is somewhat denser than agglomerate and

less dense than ignimbrite, we arrived at the value of 2.15 g/cm^3 for density of conglomerate.

Regarding the density of the basement complex, 2.65 g/cm^3 was used because Upper Cretaceous andesitic lava and pyroclastics are the main component. For quartz diorite of the intrusive bodies, 2.65 g/cm^3 of the Upper Cretaceous System was used. At first, calculation was carried out using 2.65 g/cm^3 for diorite porphyry (the section A－A'), but the calculated gravity anomaly did not agree with the measured values and finally 2.67 g/cm^3 was decided to be the appropriate value. The measured density of quartz porphyry and granodiorite samples is about 2.50 g/cm^3. But measured and calculated gravity anomalies of the Quebrada Camarones of the section B－B' and the south of the Quebrada Camerones in the section A－A' do not agree unless extremely small bodies are assumed or higher density is used. Thus density values higher than the measured values were used.

(1) Section A－A'

This section joins the northwestern part of the survey area to the southeastern part. High gravity anomaly occurs on both ends and low anomaly in the central part of this section. Basement complex is exposed in a very narrow zone of the Quebrada Vitor in the northwest and near Esquiña and on the south of Quebrada Camarones in the eastern part. Control point for two-layer modeling was set at the diorite porphyry exposure near Esquiña.

The basement surface by two-layer analysis is close to the surface of the earth near Quebrada Vitor in the northwest with all density contrasts and agrees well with the actual geology. On the other hand, on the south of the Quebrada Camarones where basement is exposed, the calculated basement does not reach the surface of the earth and does not agree with the actual geology. The following two reasons are considered to cause this discrepancy.

① There are no stations on the south of the Quebrada Camarnes where this section passes through, and thus the gravity anomaly does not exactly reflect the geology.

② The basement complex on the south of the Quebrada Camrones has lower density compared to that of the basement near Esquiña where the control point is set.

Regarding ②, high-density diorite porphyry and diorite actually occur near Esquiña and relatively low-density granodiorite occurs on the south of the Camarones.

The thickness of the upper layer in this section is maximum near the intersection with the section C－C' and reaches 1,600m at $\Delta\rho$=0.30 g/cm^3 (2.35/2.65 g/cm^3), 1,200m at $\Delta\rho$=0.40 g/cm^3 (2.25/2.65 g/cm^3) and 1,000m at $\Delta\rho$=0.50 g/cm^3 (2.15/2.65 g/cm^3). It is difficult to

determine the appropriate density contrast for this section, but for the next section B－B' $\Delta \rho$ =0.40 g/cm^3 appears to be the most appropriate density contrast.

The relief of the basement surface by multi-layer modeling is close to the results of two-layer modeling by $\Delta \rho$ =0.40g/cm^3. The basement surface gradually lowers toward the central part of the section from the uplifted parts in the northwest and along the basin of the Quebrada Camarones. The elevation of the deepest part is calculated to be about 1,500m above sea level. The difference of elevation between the uplifted parts in the northwest and along the Quebrada Camarones and the lowest part is 500~700m.

Intrusive bodies (quartz diorite, diorite porphyry, and granodiorite) were assumed at three localities from geological data, at northwestern part, Esquiña, and southern part of the Quebrada Camarones. As quartz diorite has the same density as the Upper Cretaceous System in the vicinity, the gravity anomalies are calculated to be the same regardless of the shape of the bodies. Therefore, it is noted that the shape of the quartz diorite bodies in the figure was not important during the modeling.

Although only one quartz diorite body is shown at the uplifted part in northwest, magnetic anomaly profile shows two magnetic anomalies and there is a possibility of another quartz diorite intrusion on the northwestern side of the present intrusive body. Also magnetic anomaly profile shows the coincidence of high magnetic anomaly and diorite porphyry occurrence near Esquiña and of low magnetic anomaly and granodiorite occurrence on the south of the Quebrada Camarones.

Regarding the relation between gravity anomalies and magnetic anomalies, extremely high correlation is observed between low gravity anomaly and high magnetic anomaly in the central part of the section and between high gravity anomaly and low magnetic anomaly in the southeastern part of the section.

(2) Section B－B'

This section joins the northwestern part with the southern part of the survey area. High gravity anomalies occur at both ends of the section and low gravity anomaly occurs on the northwestern side of the central part and small high gravity anomaly on the southeastern side. Basement complex outcrops occur at three localities; near the Quebrada Vitor in the northwest at the intersection with the section A-A', in the Quebrada Camarones zone in the central part, and in the southernmost part of the area. Of the above three exposures,

control point for two-layer modeling was fixed at the granodiorite outcrop in the southernmost part where the gravity anomaly is the highest.

The basement surface by two-layer modeling is near the surface of the earth for all three-density contrasts near the Qubrada Vitor in the northwest and coincides well with the geology. On the other hand, the result of the modeling differs by the density contrast in the Quebrada Camarones zone. The basement surface is deepest at 200~400m below the surface of the earth with $\Delta \rho$ =0.30 g/cm^3, and greatly differs from the actual geology. With $\Delta \rho$ =0.40 g/cm^3, although the basement complex reaches the surface of the earth at the Quebrada Camarones, it does not reach the surface at the middle slope of the southern bank of the Quebrada Camarones where the basement complex actually is exposed. With $\Delta \rho$ =0.50 g/cm^3, the basement reaches the surface extensively close to the actual distribution of the basement complex from the south bank to the north bank of the Quebrada Camarones, but the measured and calculated gravity anomaly values do not agree in some parts.

From the above, the selection of the most probable basement surface would first eliminate the results of $\Delta \rho$ =0.30 g/cm^3. Comparing the results of the remaining $\Delta \rho$ =0.40 g/cm^3 and $\Delta \rho$ =0.50 g/cm^3, agreement with actual geologic occurrences is better with $\Delta \rho$ =0.50 g/cm^3, but $\Delta \rho$ =0.40 g/cm^3 is more appropriate with the density of the upper layer. Density contrast of $\Delta \rho$ =0.50 g/cm^3 would correspond to the average density of the upper layer of 2.15 g/cm^3, which is far below the range of inferred density, 2.23~2.35 g/cm^3 and is much too low. On the other hand, $\Delta \rho$ =0.40 g/cm^3 corresponds to the average density of 2.25 g/cm^3 for the upper layer which is within reasonable range. Thus this figure is considered to be best suited for use in two-layer modeling.

The thickness of the upper layer along this section attains maximum value near the intersection with the section C－C' and attains 1,000m with $\Delta \rho$ =0.40 g/cm^3, 1,450 m with $\Delta \rho$ =0.30 g/cm^3, and 750m with $\Delta \rho$ =0.50 g/cm^3. On the south of the Quebrada Camarones, the thickest part of the upper layer is calculated to be 600~700 m ($\Delta \rho$ =0.40 g/cm^3).

The relief of the basement surface by multi-layer modeling is close to the result of two-layer modeling with $\Delta \rho$ =0.40 g/cm^3. The basement surface which is largely uplifted at the southernmost part of the survey area gently drops toward the northwest, and after the lowest point near the intersection with the section C－C', gradually rises to the northwest. The elevation of the lowest part near the intersection with the section C－C' is about 1,600 m above sea level and the difference of elevation between the highest point in the southernmost

part reaches 1,200 m. Although it is not known accurately because of erosion and landslides, the basement was possibly uplifted locally near the Quebrada Camarones.

In this section, intrusive bodies (quartz diorite, quartz porphyry, and quartz diorite) are assumed, in accordance with geological data, at three localities, namely the northwestern part, the northern bank of the Quebrada Camarones, and the southernmost part of the area. The quartz diorite bodies at both ends of the section do not have density contrast with the rocks of the vicinity as in the case of section A−A', and thus the shape of the figure is not the result of modeling.

A small low gravity anomaly occurs at the central part of a local high gravity anomaly extending on both banks of the Quebrada Camarones. This low gravity coincides with high local magnetic anomaly and corresponds with the occurrence of quartz porphyry. Quartz porphyry has lower density compared to the basement rocks in the vicinity and is appropriate to be expressed as a local low gravity. But if we assume a density of 2.50 g/cm^3 for the quartz porphyry, the intrusive body will have to be extremely small for the calculated and measured gravity anomalies to coincide. Assuming a density of 2.55 g/cm^3 draws the shape of the body in the figure, but the calculated and measured values do not approximate sufficiently. For the two values to approximate closely, either the intrusive body should be small or use density value closer to 2.65 g/cm^3. But since two-dimensional assumption does not describe the body sufficiently, agreement of details would not be appropriate. It is also possible that the small size of the intrusive body indicates that the section passes through the peripheral parts of the rock. Residual map of Figure 2-2-12 indicates eastward expansion of the local low gravity anomaly, and the center of the quartz porphyry body may be located to the east of the section.

High correlation is observed between low gravity anomalies and high magnetic anomalies on the northwestern side of the central part of the magnetic anomaly profile. This is similar to the section A−A'. The high gravity anomalies at both ends of the section do not coincide with low magnetic anomalies and this is interpreted to be the effect of the high magnetic anomalies corresponding to the intrusive body.

(3) Section C−C'

This section joins the western part with the eastern part of the survey area. High gravity anomalies occur at both ends and low gravity anomaly in the central part. Basement rocks are not exposed along the section.

The basement surface by two-layer modeling is close to the surface of the earth at the high gravity anomaly zone in the west regardless of the density contrast. Lowest Neogene conglomerate is confirmed in the vicinity and the result is harmonious with the actual geologic occurrences. On the other hand, shallowest depth of about 300m is calculated for the basement surface in the high gravity anomaly zone in the east near Saguara. The upper layer is thickest near the intersection with the section A−A' and it is calculated to be about 1,200m with $\Delta \rho$ =0.40 g/cm^3 .

The basement surface relief by multi-layer modeling is similar to the calculated results of two-layer modeling with $\Delta \rho$ =0.40 g/cm^3. The basement surface is shallow in the western part of the section, but the scale of uplifting is larger in the eastern part, and the difference of elevation of the basement surface in the eastern uplifted part and the central sunken part is 1,100 m.

2-2-5 Results of three-dimensional analysis

Three-dimensional two-layer modeling was carried out in order to clarify the relief of the basement surface and the thickness of the overlying volcanic rocks. The density contrast between the basement rocks and the upper layers (volcanic rocks) was assumed to be $\Delta \rho$ =0.40 g/cm^3 , and the control point was fixed in the basement exposure (diorite) near Esquiña.

(1) Relief of the basement surface

The results of three-dimensional two-layer modeling with $\Delta \rho$ =0.40 g/cm^3 are shown in Figure 2-2-19. The contours indicate the elevation of the basement surface.

Figure 2-2-19 shows that the basement surface of the survey area is relatively high in the southeastern and eastern part and is low along the Quebrada Camarones. Some of the southeasternmost and easternmost parts are more than 3,000m above sea level and further rises to the southeast. The basement surface drops westward steeply for about 400m, during a short distance of 2km from 442km to 440km in UTM coordinates on the north of the Quebrada Camarones, large relief exceeding 300m do not occur to the west of this zone. The lowest basement surface aside from the Quebrada Camarones is in the zone from middle stream of Quebrada Sucuna to middle Quebrada Vitor and in the lower reaches of Quebrada Sucuna, and the elevation is calculated to be 1,700~1,800m.